



Early Pliocene increase in thermohaline overturning: A precondition for the development of the modern equatorial Pacific cold tongue

Silke Steph,^{1,2,3} Ralf Tiedemann,¹ Matthias Prange,⁴ Jeroen Groeneveld,⁴
Michael Schulz,⁴ Axel Timmermann,⁵ Dirk Nürnberg,⁶ Carsten Rühlemann,⁷
Cornelia Saukel,¹ and Gerald H. Haug^{3,8}

Received 28 May 2008; revised 29 July 2009; accepted 15 October 2009; published 15 April 2010.

[1] Unraveling the processes responsible for Earth's climate transition from an "El Niño-like state" during the warm early Pliocene into a modern-like "La Niña-dominated state" currently challenges the scientific community. Recently, the Pliocene climate switch has been linked to oceanic thermocline shoaling at ~3 million years ago along with Earth's final transition into a bipolar icehouse world. Here we present Pliocene proxy data and climate model results, which suggest an earlier timing of the Pliocene climate switch and a different chain of forcing mechanisms. We show that the increase in North Atlantic meridional overturning circulation between 4.8 and 4.0 million years ago, initiated by the progressive closure of the Central American Seaway, triggered overall shoaling of the tropical thermocline. This preconditioned the turnaround from a warm eastern equatorial Pacific to the modern equatorial cold tongue state about 1 million years earlier than previously assumed. Since ~3.6–3.5 million years ago, the intensification of Northern Hemisphere glaciation resulted in a strengthening of the trade winds, thereby amplifying upwelling and biogenic productivity at low latitudes.

Citation: Steph, S., R. Tiedemann, M. Prange, J. Groeneveld, M. Schulz, A. Timmermann, D. Nürnberg, C. Rühlemann, C. Saukel, and G. H. Haug (2010), Early Pliocene increase in thermohaline overturning: A precondition for the development of the modern equatorial Pacific cold tongue, *Paleoceanography*, 25, PA2202, doi:10.1029/2008PA001645.

1. Introduction

[2] Understanding the causal chain of Pliocene climate forcing may help to improve predictions of future climate change, including the ultimate role of the ocean circulation in a globally warmer world [Jansen *et al.*, 2007]. During the Pliocene warm period from ~5.5 to ~3 Ma, mean global surface temperatures were ~3°C warmer than today, atmospheric CO₂ concentrations were close to modern ones [Foster *et al.*, 2009], the modern Northern Hemisphere ice

cap was absent, and sea level was ~25 m higher than today [e.g., Raymo *et al.*, 1996; Dowsett *et al.*, 1999; Ravelo *et al.*, 2004; Mudelsee and Raymo, 2005]. Growing evidence from early Pliocene paleoclimate data suggests that sea surface temperatures (SST) in the eastern equatorial Pacific (EEP) cold tongue were similar to those of the western tropical Pacific Warm Pool [Chaisson and Ravelo, 2000; Molnar and Cane, 2002; Ravelo *et al.*, 2004; Wara *et al.*, 2005]. Warm surface water, a deep thermocline, and low biogenic productivity characterized the low-latitude to midlatitude upwelling regions [Fedorov *et al.*, 2006; Dekens *et al.*, 2007].

[3] The timing and mechanisms for the development of the modern EEP cold tongue state have so far been linked to the mid-Pliocene intensification of Northern Hemisphere glaciation (NHG) [Fedorov *et al.*, 2006]. According to a recent hypothesis [Fedorov *et al.*, 2006], cooling of the deep ocean, associated with enhanced oceanic heat loss at high latitudes and a balanced increase in heat gain at low latitudes, caused the tropical thermocline to shoal. This thermocline shoaling has been proposed to reach a critical threshold at ~3 Ma, allowing trade winds to bring cooler waters to the surface in equatorial and coastal upwelling zones.

[4] However, there is also evidence that cooling of the upwelling regions off California [Fedorov *et al.*, 2006; Dekens *et al.*, 2007; Liu *et al.*, 2008; Brierley *et al.*, 2009], West Africa [Marlow *et al.*, 2000] and within the EEP cold tongue [Lawrence *et al.*, 2006; Dekens *et al.*, 2007]

¹Alfred Wegener Institute for Polar and Marine Research, Bremerhaven, Germany.

²Geology and Geophysics Department, Woods Hole Oceanographic Institution, Woods Hole, Massachusetts, USA.

³Now at DFG–Leibniz Center for Surface Process and Climate Studies, Institute for Geosciences, Potsdam University, Potsdam, Germany

⁴MARUM–Center for Marine Environmental Sciences and Department of Geosciences, University of Bremen, Bremen, Germany.

⁵IPRC, SOEST, University of Hawai'i at Mānoa, Honolulu, Hawaii, USA.

⁶Leibniz Institute of Marine Sciences at University of Kiel (IFM-GEOMAR), Kiel, Germany.

⁷Bundesanstalt für Geowissenschaften und Rohstoffe, Hannover, Germany.

⁸Geological Institute, Department of Earth Sciences, ETH Zurich, Zurich, Switzerland.

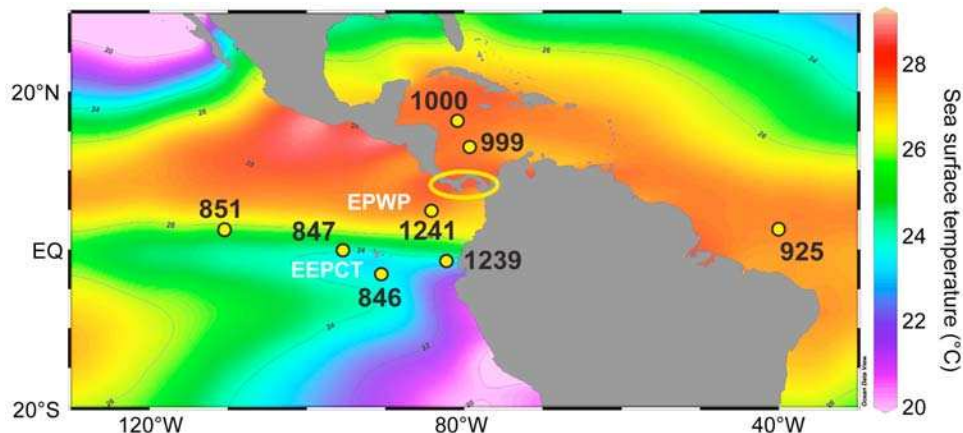


Figure 1. Map showing modern annual sea surface temperatures in the tropical eastern Pacific and western Atlantic/Caribbean (NODC, 2001 [Conkright et al., 2002]). Yellow dots show the locations of ODP sites discussed in this study (Site 846, 3°06'S, 90°49'W, 3296 m water depth; Site 847, 0°12'N, 95°19'W, 3334 m water depth; Site 851, 2°46'N, 110°34'W, 3761 m water depth; Site 925, 4°12'N, 43°29'W, 3041 m water depth; Site 999, 12°45'N, 78°44'W, 2828 m water depth; Site 1000, 16°33'N, 79°52'W, 916 m water depth; Site 1239, 0°40'S, 82°05'W, 1414 m water depth; Site 1241, 5°51'N, 86°27'W, 2027 m water depth). The ellipse is indicating the final openings of the Central American Seaway. EEPCT, eastern equatorial Pacific cold tongue; EPWP, East Pacific Warm Pool.

started more than 600 kyr earlier (~4.5–3.6 Ma). Here, we present new proxy data that strongly corroborate an early development of the EEP cold tongue. This timing questions the intensification of NHG as exclusive forcing mechanism. Instead, it suggests an additional link to the early Pliocene threshold in the closure history of the Central American Seaway (CAS), which was associated with an increase in Atlantic meridional overturning circulation (AMOC) [e.g., Haug and Tiedemann, 1998]. Using Pliocene proxy data as well as results from a coupled climate model, we test the hypothesis that changes in the strength of the AMOC can trigger global adjustments of the thermocline depth (TCD). Such a link has been proposed by theoretical and modeling studies [e.g., Huang et al., 2000; Timmermann et al., 2005], but has so far not been observed or verified by proxy data.

2. Material and Methods

2.1. Sample Material

[5] We present new Pliocene planktonic foraminiferal $\delta^{18}\text{O}$ and Mg/Ca-derived temperatures, alkenone (U_{37}^K) SSTs, opal accumulation rates, and benthic foraminiferal $\delta^{13}\text{C}$ from tropical eastern Pacific Ocean Drilling Program (ODP) sites 1239 (0°40'S, 82°05'W, 1414 m water depth) and 1241 (5°51'N, 86°27'W, 2027 m water depth) [Mix et al., 2003] as well as from Caribbean ODP sites 999 (12°45'N, 78°44'W, 2828 m water depth) and 1000 (16°33'N, 79°52'W, 916 m water depth) [Sigurdsson et al., 1997] (Figure 1). The preservation of foraminiferal carbonate shells is generally good according to the relatively shallow site locations well above the lysocline [Sigurdsson et al., 1997; Mix et al., 2003]. The proxy records span the time interval from ~2.1 Ma to 5.5 Ma. Pliocene age models for all sites are based on orbital tuning (see Tiedemann et al. [2007] for tropical eastern Pacific sites 1239 and 1241 and Haug and

Tiedemann [1998] and Steph et al. [2006a] for Caribbean sites 999 and 1000).

2.2. Stable Isotope Measurements

[6] The samples were freeze-dried and washed through a 63 μm mesh. For $\delta^{18}\text{O}$ measurements on planktonic foraminifera, ten to fifteen specimens of *Neogloboquadrina dutertrei* (thermocline dweller) were selected from the 315–400 μm size fraction of samples from Caribbean sites 999 and 1000. Due to the lower amount of planktonic foraminifera in samples from equatorial eastern Pacific Site 1239, we picked ten to fifteen specimens of *Globigerinoides sacculifer* (mixed layer dweller) and *Globorotalia tumida* (habitat near the bottom of the photic zone) from the >250 μm size fraction. For benthic $\delta^{13}\text{C}$ measurements at Site 1000, we selected one to five tests of the epibenthic foraminifera *Cibicidoides wuellerstorfi* (>315 μm). Prior to analysis, visibly contaminated specimens were slightly crushed and ultrasonically cleaned with methanol. The excess liquid and mud were siphoned off and the samples were dried at 60°C.

[7] Stable isotope analyses on planktonic and epibenthic foraminifera were carried out at IFM-GEOMAR (Kiel), using either a Finnigan Delta-Plus-Advantage mass spectrometer coupled to a Finnigan Gas Bench II (with analytical precision better than ± 0.07 ‰ for $\delta^{18}\text{O}$ and better than ± 0.05 ‰ for $\delta^{13}\text{C}$; $\pm 1\sigma$), or a Finnigan MAT 252 mass spectrometer with automated Kiel carbonate preparation device (with analytical precision better than ± 0.07 ‰ for $\delta^{18}\text{O}$ and ± 0.04 ‰ for $\delta^{13}\text{C}$; $\pm 1\sigma$). Both machines were intercalibrated using a house standard, which was calibrated to the National Bureau of Standards NBS-19. The ratios of $^{18}\text{O}/^{16}\text{O}$ and $^{13}\text{C}/^{12}\text{C}$ are reported with reference to the Pee Dee Belemnite (PDB) standard.

2.3. Mg/Ca Analyses

[8] For Mg/Ca measurements, 20–25 specimens of *N. dutertrei* (sites 999, 1000) and *G. tumida* (Site 1239) were picked from the same size fraction as used for stable isotope analyses. Specimens visibly contaminated by ferromanganese oxides were not selected for analysis. After gentle crushing, the samples were cleaned according to the cleaning protocol for Mg/Ca of *Barker et al.* [2003]. To remove clays, the samples were rinsed four to six times with distilled deionized water and twice with methanol (suprapure) with ultrasonical cleaning steps (2 to 3 min) after each rinse. Subsequently, samples were treated with a hot (97°C) oxidizing 1% NaOH/H₂O₂ solution (10 ml 0.1 N NaOH (analytical grade); 100 μ l 30% H₂O₂ (suprapure)) for 10 min to remove organic matter. Every 2.5 min, the vials were rapped on the bench top to release any gaseous buildup. After 5 min, the samples were placed in an ultrasonic bath for a few seconds to maintain contact between reagent and sample. This treatment was repeated after refreshment of the oxidizing solution. The remaining oxidizing solution was removed during three rinsing steps with distilled deionized water. After transferring the samples into clean vials, a weak acid leach with 250 μ l 0.001 M HNO₃ (subboiled distilled) was applied with 30 s ultrasonic treatment and subsequent two rinses with distilled deionized water. After cleaning, the samples were dissolved in 0.075 M nitric acid (HNO₃) (subboiled distilled) and diluted several times, until all samples obtained calcium concentrations in the range of 30–70 ppm.

[9] Analyses were performed on an ICP-AES (ISA Jobin Yovin-Spex Instruments S.A. GmbH) at IFM-GEOMAR (Kiel) or on a simultaneous, radially viewing ICP-OES (Ciros CCD SOP, Spectro A. I., Germany) at the Institute of Geosciences (Kiel University, Germany). The long-term precision of the Mg/Ca analyses estimated from an internal laboratory standard was 0.1%. Replicate analyses on the same samples, which were cleaned and analyzed during different sessions, showed a standard deviation of 0.09 mmol/mol, introducing a temperature error of about 0.5°C.

2.4. Calculation of Mg/Ca-Derived Paleotemperatures

[10] For this study, *G. sacculifer* Mg/Ca temperatures were calculated using the *Dekens et al.* [2002] Mg/Ca temperature calibration for *G. sacculifer* with core-depth-based dissolution corrections for the Pacific (Site 1241) and for the Atlantic (sites 999, 1000). *N. dutertrei* Mg/Ca ratios from Caribbean sites 999 and 1000 were converted into temperature using the *Dekens et al.* [2002] Mg/Ca temperature calibration for *N. dutertrei* with a core-depth-based dissolution correction for the Atlantic. We used the *Anand et al.* [2003] multispecies Mg/Ca temperature calibration to calculate *G. tumida* Mg/Ca paleotemperatures at Pacific sites 1239 and 1241 and we included the *Dekens et al.* [2002] core-depth-based Pacific dissolution correction for *G. sacculifer*, because species-specific dissolution corrections for *G. tumida* are not available for the Pacific.

$$\text{Mg/Ca} = 0.38 \exp(0.09[T - 0.36(\text{core depth in km}) - 2.0^\circ\text{C}]) \quad (1)$$

[11] Yet we are aware that Mg/Ca *G. tumida* might have a different sensitivity to carbonate dissolution than Mg/Ca *G. sacculifer*, which would in turn affect the resulting absolute *G. tumida* Mg/Ca temperature estimates. Absolute Mg/Ca temperature estimates of course depend on the selection of Mg/Ca temperature calibrations used for the calculations, but the relative changes in vertical temperature gradients are robust regardless of which calibration is used. Our conclusions, which are mainly based on the evolutionary long-term changes of vertical temperature gradients between the mixed layer and the bottom of the photic zone, would therefore not be affected by the application of other Mg/Ca temperature calibrations.

2.5. Calculation of Opal Accumulation Rates

[12] To estimate opal accumulation rates at Site 1239, we quantified the concentrations of biogenic silica (opal) for 15 samples by using the automated leaching method according to *Müller and Schneider* [1993]. The opaline material was extracted from the dry and ground bulk sediment by sodium hydroxide at ~85°C for ~45 min. The leaching solution was continuously analyzed for dissolved silicon by molybdate blue spectrophotometry. The *DeMaster* [1981] mineral correction was consequently applied. The excellent linear correlation of opal concentrations with shipboard grape density data [*Mix et al.*, 2003] ($R = 0.8$) allowed for the calculation of a high-resolution opal percentage record. Mass accumulation rates ($\text{g cm}^{-2} \text{ kyr}^{-1}$) were then calculated using the sedimentation rate (in cm kyr^{-1}) between age control points [*Tiedemann et al.*, 2007], dry bulk density data calculated from grape density and shipboard physical properties data [*Mix et al.*, 2003], and the opal concentrations (%).

2.6. Alkenone Analysis

[13] Samples of 2 g freeze-dried and homogenized sediment were mixed with an internal standard and ultrasonically extracted for 3 min (UP200H ultrasonication disrupter probe; S3 micropoint, amplitude 0.5, pulse 0.5), using successively less polar mixtures of methanol and methylene chloride (CH₃OH, CH₃OH/CH₂Cl₂ 1:1, CH₂Cl₂). After centrifuging, the supernatants were combined, desalted with deionized water, dried with Na₂SO₄ and rotary evaporated to complete dryness. The residues were dissolved in CH₂Cl₂ and additionally purified using a silica cartridge (Varian Bond Elut; 1CC/100 mg). To eliminate interference with wax esters, the clean extracts were hydrolyzed with 0.1 N KOH in Methanol (90/10 CH₃OH/H₂O) at 80°C for 2 h, and the neutral fraction containing the alkenones was obtained by partitioning into hexane. Finally, the extracts were concentrated under N₂ and taken up in 25 μ l of the 1:1 CH₃OH/CH₂Cl₂ mixture. Gas chromatography was performed using a HP5890 series II gas chromatograph equipped with a split/splitless injector, a 60 m \times 0.32 mm \times 0.1 μ m nonpolar fused silica capillary column DB-5MS and flame ionization detector. An aliquot of 3 μ l was injected in split mode (one tenth) with helium as the carrier gas. The oven temperature was programmed from 50°C to 250°C at 25°/min, 250°C to 290°C at 1°/min and a final heating from 290°C to 310°C at 30°/min. Compounds were quantified using octacosane acid methyl ester as an internal standard and the relative response

of the C38 n-alkane. The ketone unsaturation index $U_{37}^{K'}$ was converted to temperature according to *Conte et al.* [2006]:

$$T(^{\circ}\text{C}) = -0.957 + 54.3(U_{37}^{K'}) - 52.9(U_{37}^{K'})^2 + 28.3(U_{37}^{K'})^3. \quad (2)$$

[14] We applied the nonlinear $U_{37}^{K'}$ /temperature calibration of *Conte et al.* [2006] because it is based on alkenones from surface water particulates collected in the world ocean (i.e., the natural environment of the alkenone producers) and associated temperatures measured at sampling depth. Moreover, this calibration accounts for the asymptotic behavior of $U_{37}^{K'}$ at the warmest SSTs. The analytical precision ($\pm 1\sigma$) based on duplicates and multiple extractions of a sediment sample used as an internal laboratory reference sample was better than $0.003 U_{37}^{K'}$ units or 0.1°C .

2.7. Climate Model Experiments

[15] For our sensitivity experiments, we used the global atmosphere-ocean model ECBILT-CLIO version 3. The coupled model derives from the atmosphere model ECBILT [*Opsteegh et al.*, 1998] and the ocean/sea ice model CLIO [*Goosse and Fichefet*, 1999]. The atmospheric component solves the quasi-geostrophic equations and ageostrophic correction terms in T21 resolution using three layers. The primitive equation, free surface ocean component has a horizontal resolution of 3 degrees and 20 levels in the vertical. It is coupled to a thermodynamic-dynamic sea ice model with viscous plastic rheology. There is no local flux correction in ECBILT-CLIO. However, precipitation over the Atlantic and Arctic basins is reduced by 8.5% and 25%, respectively, and homogeneously redistributed over the North Pacific. The implementation of this regional flux adjustment considerably improves the simulation of the present-day climate and produces a realistic AMOC. Its reliability in the simulation of other climates than the present one, however, is elusive. For the sensitivity studies presented in this paper, the potential errors in surface hydrography and AMOC that are induced by the flux adjustment are acceptable since we are interested in the qualitative relationship between the AMOC and the thermocline, rather than in precise numbers. More information about the model and a complete list of references is available at <http://www.knmi.nl/onderzk/CKO/ecbilt-papers.html>.

[16] Beside a 5000 years control run (experiment CTL), simulating the present-day (preindustrial) climate, we conducted an experiment with open Central American Seaway (experiment CAS) and a freshwater hosing experiment (experiment OFF). These experiments were designed to elucidate the relationship between AMOC and tropical TCD. The freshwater hosing is a convenient method to shut off the AMOC, providing an estimate for the maximum response of tropical TCD to pure AMOC slowing. We note that we do not imply corresponding meltwater events in the early Pliocene.

[17] In experiment CAS, the Panama Seaway has a sill depth of 700 m and is defined on three velocity grid points,

corresponding to a width of approximately 1000 km. All other boundary conditions are the same as in the control run. Therefore, experiment CAS should be viewed as a sensitivity study to elucidate tropical thermocline dynamics rather than a simulation of early Pliocene climate. In experiment OFF Panama is closed, but NADW formation is completely shut off by an anomalous freshwater input to the North Atlantic (0.5 Sv between 50°N and 70°N). In both experiments CAS and OFF, the model was integrated another 2250 years to reach a new equilibrium, starting from the control run's final state as initial condition. Model results presented in this paper are annual averages determined from the last 50 years of each experiment.

[18] Generally, the thermocline is defined as the depth at which the vertical temperature gradient is at a maximum. In a numerical ocean model such as CLIO, the search for this maximum would always result in thermocline depths that correspond exactly to the depths of grid points (in ECBILT-CLIO these are located at 5 m, 16 m, 29 m, 45 m, 65 m, 90 m, 122 m, etc.). Hence, changes that are smaller than the vertical grid spacing could not be observed when using the maximum temperature gradient for the calculation of TCD. Therefore, alternative indicators for TCD are generally used in numerical models. As an indicator for tropical TCD, we use the depth of the 20°C isotherm (the depth of an isotherm is not bound to the grid spacing; an isotherm can well reside between two grid points in the vertical and its depth can easily be found by linear interpolation of the gridded temperature field). In both observational data and the ECBILT-CLIO climate model, the depth of the maximum temperature gradient is almost identical to the depth of the 20°C isotherm in the central (~ 150 m) and eastern (less than 50 m on average) equatorial Pacific.

3. Results

3.1. Equatorial Eastern Pacific Site 1239

3.1.1. Planktonic $\delta^{18}\text{O}$ and Mg/Ca Paleotemperature Records

[19] The $\delta^{18}\text{O}$ record of the mixed layer dweller *G. sacculifer* as well as $\delta^{18}\text{O}$ and Mg/Ca temperature records of the deep dweller *G. tumida* (habitat close to the bottom of the photic zone [*Ravelo and Fairbanks*, 1992; *Ravelo and Andreasen*, 1999]) serve to reconstruct Pliocene changes in upper ocean stratification at equatorial eastern Pacific Site 1239 (Figure 2a). Small (large) surface/subsurface temperature differences, and hence small (large) $\delta^{18}\text{O}$ differences between shallow- and deep-dwelling planktonic foraminifera indicate a deep (shallow) thermocline [e.g., *Ravelo and Fairbanks*, 1992; *Ravelo and Andreasen*, 1999; *Steph et al.*, 2009].

[20] At Site 1239, $\delta^{18}\text{O}$ values of the mixed layer dweller *G. sacculifer* remained relatively constant between 5.0 and 3.9 Ma (average $\delta^{18}\text{O}$ of -1.1‰). From 3.9 to 2.7 Ma, the $\delta^{18}\text{O}$ values of *G. sacculifer* increased by $\sim 0.4\text{‰}$ (average $\delta^{18}\text{O}$ of -0.7‰ between 2.7 and 2.9 Ma) with a major step around ~ 3.7 Ma (Figure 2a). The Mg/Ca temperature and $\delta^{18}\text{O}$ records of the deep dweller *G. tumida*, however, suggest larger temperature changes at the bottom of the photic zone. Average *G. tumida* $\delta^{18}\text{O}$ values increased by

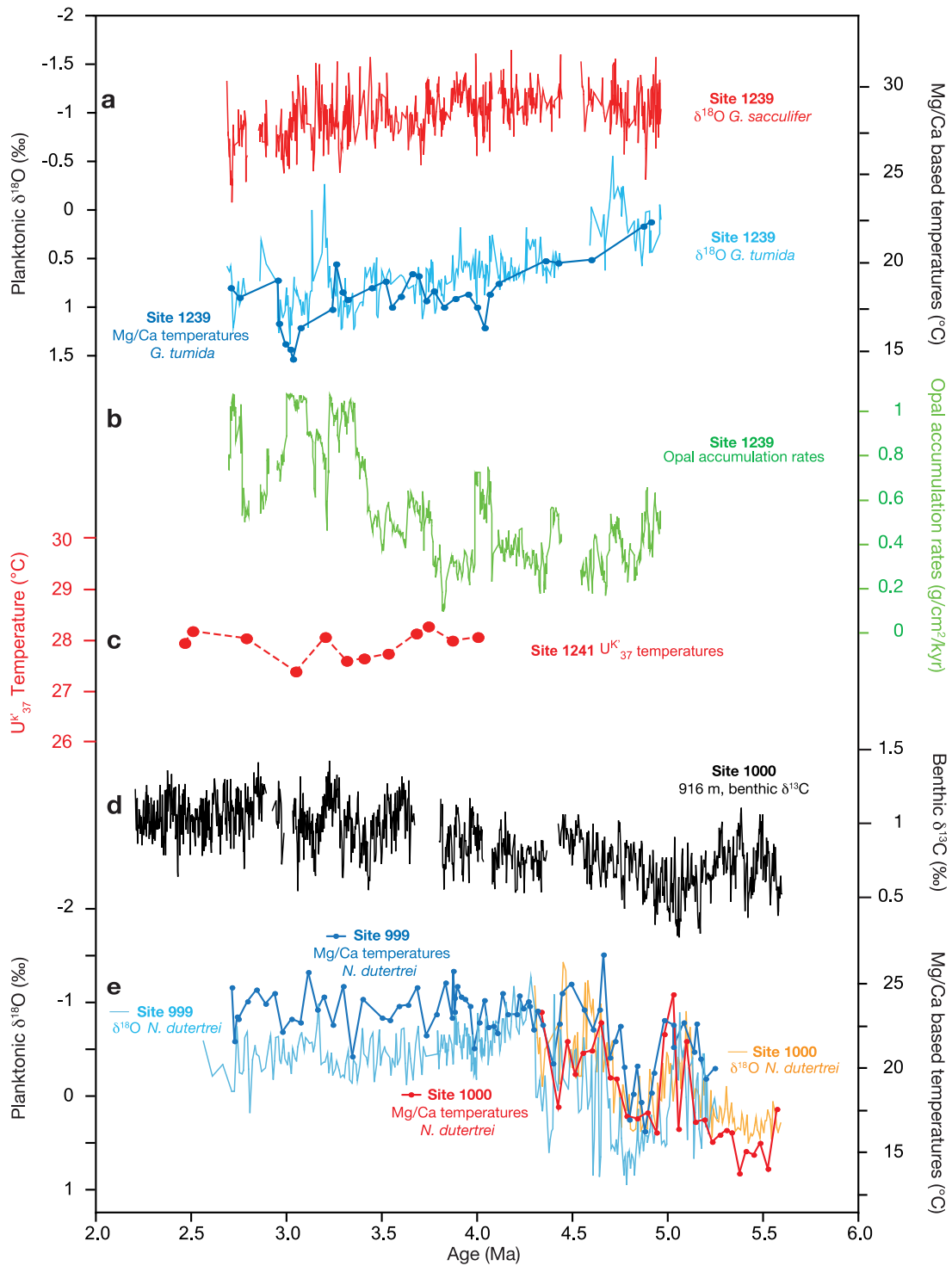


Figure 2. New proxy data presented in this study, spanning the time interval from ~5.6 Ma to 2.1 Ma. (a) *G. sacculifer* $\delta^{18}\text{O}$ data (red line), *G. tumida* $\delta^{18}\text{O}$ data (light blue line) and Mg/Ca temperature data (dark blue) from equatorial eastern Pacific ODP Site 1239. (b) Biogenic opal accumulation rates, Site 1239 (green line). (c) U^{K}_{37} sea surface temperature data from tropical eastern Pacific Site 1241 (red). (d) Epibenthic $\delta^{13}\text{C}$ record from Caribbean Site 1000 (*C. wuellerstorfi*, black line). (e) The $\delta^{18}\text{O}$ records of the thermocline dweller *N. dutertrei* (dextral variety) from Caribbean sites 999 (light blue) and 1000 (orange) and Mg/Ca temperature records of *N. dutertrei* (dextral variety) from sites 999 (dark blue) and 1000 (red).

~0.5‰ between 4.8 and 4.0 Ma, and by an additional ~0.3‰ between 3.8 and 3 Ma (Figure 2a). The low-resolution *G. tumida* Mg/Ca temperature record at Site 1239 shows a similar pattern; temperatures decrease by ~5°C during the early Pliocene, with a major step between ~4.8 and ~4.0 Ma (Figure 2a). This subsurface cooling and the increasing $\delta^{18}\text{O}$ gradient between the mixed layer and the bottom of the photic zone point to a TCD decrease at Site 1239 during the early Pliocene. Between 4.0 and 2.7 Ma, *G. tumida* Mg/Ca temperatures remained relatively stable, except for a pronounced cool interval between 3.3 and 3.0 Ma (Figure 2a).

3.1.2. Biogenic Opal Accumulation Rates

[21] We use biogenic opal accumulation rates calculated from equatorial eastern Pacific Site 1239 shipboard grape density data [Mix *et al.*, 2003] as an estimate for changes in diatom productivity (Figure 2b). Between 5.0 and 3.6 Ma, opal accumulation rates were low (on average ~0.4 g cm⁻² kyr⁻¹) and the variability was relatively small, except for a short interval with higher opal accumulation rates (up to 0.7 g cm⁻² kyr⁻¹) around 4.0 Ma. Between 3.6 and 3.5 Ma, opal accumulation rates at Site 1239 doubled rapidly to average values of ~0.8 g cm⁻² kyr⁻¹ (reaching maximum values of 1.05 g cm⁻² kyr⁻¹), suggesting a distinct increase of diatom productivity at Site 1239 after 3.6–3.5 Ma (Figure 2b).

3.2. Tropical Eastern Pacific Site 1241

[22] We measured a low-resolution U_{37}^{K} record spanning the time interval from 4.0 to 2.5 Ma in order to get hold of SST changes in the upper 10 m of the water column, the preferred habitat of alkenone-producing coccolithophores. The Site 1241 U_{37}^{K} temperatures vary between 27.4°C and 28.3°C and show no long term trend (Figure 2c), suggesting that Pliocene SSTs in the uppermost water column were relatively constant in time and only slightly warmer than today (modern SSTs are ~27.0°C at the 4 Ma paleolocation and 27.4°C at the 2 Ma paleolocation of Site 1241).

3.3. Caribbean Sites 999 and 1000

3.3.1. Site 1000 Benthic $\delta^{13}\text{C}$ Record (*C. wuellerstorfi*)

[23] The $\delta^{13}\text{C}$ record of the epibenthic foraminifer *C. wuellerstorfi* serves as a proxy for changes in deep water ventilation [e.g., Zahn *et al.*, 1986; McCorkle and Keigwin, 1994], because the $\delta^{13}\text{C}$ of seawater is closely linked to nutrient and oxygen contents, whereas higher $\delta^{13}\text{C}$ values indicate lower nutrient contents and better ventilation [Kroopnick, 1985]. Caribbean Site 1000 (916 m water depth) provides information about ventilation changes at the Atlantic intermediate water level. Benthic $\delta^{13}\text{C}$ at Site 1000 decreased during the earliest Pliocene, reaching the lowest level between ~5.2 Ma and 4.9 Ma (average $\delta^{13}\text{C} = 0.6$ ‰) (Figure 2d). Between ~4.9 and 3.6 Ma, Site 1000 benthic $\delta^{13}\text{C}$ increased to average values of ~1.1‰. These high $\delta^{13}\text{C}$ persisted until 2.2 Ma. The overall early Pliocene $\delta^{13}\text{C}$ trend suggests an increase in intermediate water ventilation (Figure 2d).

3.3.2. *N. dutertrei* $\delta^{18}\text{O}$ and Mg/Ca Paleotemperature Records

[24] We use $\delta^{18}\text{O}$ and Mg/Ca temperature records measured on the thermocline dweller *N. dutertrei* in order to

reconstruct Pliocene Caribbean subsurface temperature changes, because the deep dweller *G. tumida* is absent in the Pliocene sections of sites 999 and 1000. The subsurface temperature development was very similar at both Caribbean sites (Figure 2e). Between 4.8 and 4.3 Ma, average $\delta^{18}\text{O}_{N. dutertrei}$ decreased by more than 1‰, whereas the *N. dutertrei* Mg/Ca temperature records indicate a synchronous subsurface temperature increase of ~4°C. Between 4.3 and 4.0 Ma, $\delta^{18}\text{O}_{N. dutertrei}$ increased while *N. dutertrei* Mg/Ca temperatures stayed stable, hinting to an increase in Caribbean subsurface salinity (Figure 2e). After 4.0 Ma, small long-term variations in the $\delta^{18}\text{O}$ and Mg/Ca temperature records of *N. dutertrei* indicate no major change in thermocline temperature and/or salinity at Caribbean Site 999.

3.4. Model Results

[25] Introducing a Panama Seaway in experiment CAS results in a mean total volume transport of 14 Sv (1 Sv = 10⁶ m³ s⁻¹) from the Pacific into the Atlantic over the entire depth (700 m) of the strait. The inflow of relatively fresh Pacific surface water masses into the Atlantic reduces the salinity contrast between the two oceans and, as a result, the AMOC decreases. This is a robust result which has already been found in previous modeling studies and which is essentially independent of other boundary conditions [cf. Maier-Reimer *et al.*, 1990; Klocker *et al.*, 2005; Lunt *et al.*, 2008]. In our model, convection in the Labrador Sea, and hence UNADW formation, stops. The strength of the AMOC (measured by the net export of NADW to the Southern Ocean) is 15 Sv in the control run and 9 Sv in experiment CAS [cf. Prange and Schulz, 2004]. Figure 3a illustrates global changes in the depth of the 20°C isotherm (which is a good indicator for tropical TCD; see above) in response to the closure of the CAS. The pattern indicates an overall decrease in tropical TCD, except for the Caribbean, where the thermocline deepens (Figure 3a). Except for the Caribbean, the global pattern of TCD change between experiments CTL and OFF provides a very similar picture, albeit with a larger magnitude of thermocline shoaling in most areas of the world ocean as compared to experiment CAS (Figure 3b).

4. Discussion

4.1. Changes in Tropical Eastern Pacific Thermocline Depth

[26] We use new and previously published Mg/Ca temperature records and $\delta^{18}\text{O}$ values of the shallow-dwelling planktonic foraminifer *G. sacculifer* and of the deep dweller *G. tumida* to assess Pliocene variations in tropical eastern Pacific TCD (Figure 4). ODP Site 1241 is located at ~6°N close to the present-day Intertropical Convergence Zone (ITCZ) at the southern edge of the East Pacific Warm Pool, where upwelling is absent and tropical wind stress convergence is largest (doldrums; Figure 1). It has therefore an ideal position to monitor oceanic adjustments in TCD. Pliocene alkenone-derived SSTs at Site 1241 were high and relatively constant (~28°C; Figure 4a) and temperature fluctuations derived from Mg/Ca_{*G. sacculifer*} were also small (~2°C) [Groeneveld *et al.*, 2006] (Figure 4a). Pliocene

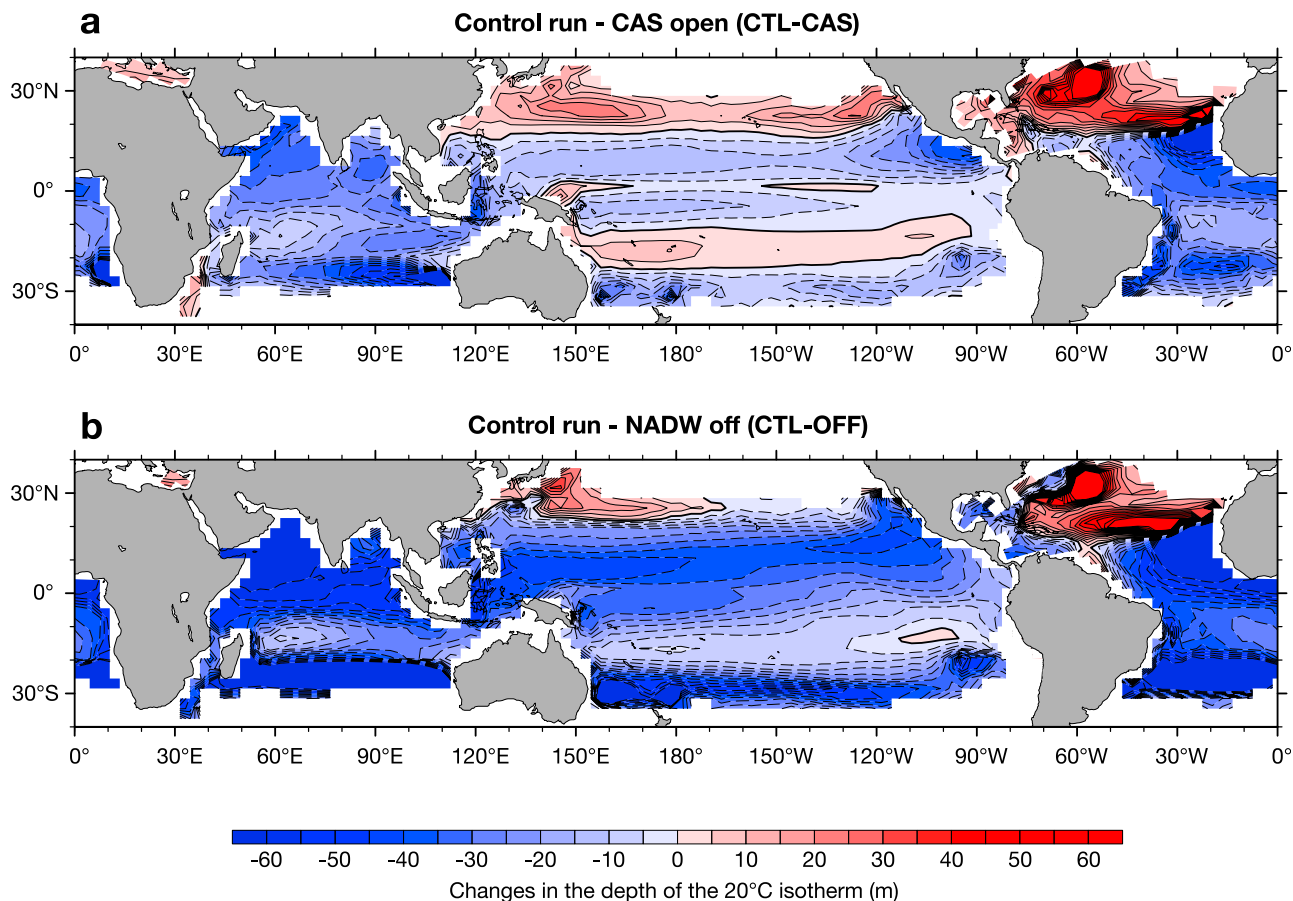


Figure 3. Differences in the depth of the 20°C isotherm (annual mean) between the present-day control run CTL and (a) experiment CAS with open Central American Seaway and (b) experiment OFF with NADW formation shut off completely by a strong anomalous freshwater input to the North Atlantic.

Mg/Ca_{G. sacculifer} paleotemperature estimates at Site 1241 are on average ~1°C lower than alkenone-derived temperatures if using the *Dekens et al.* [2002] *G. sacculifer* calibration with Pacific dissolution correction factors for Mg/Ca temperature calculations. This relatively small temperature offset may either be related to differences in seasonality or to the fact that U₃₇^K provides SST's within the uppermost water column (~0–10 m water depth) while Mg/Ca_{G. sacculifer} displays mixed layer temperatures (the modern average calcification depth of *G. sacculifer* in the Panama Basin is ~30–50 m [e.g., *Fairbanks et al.*, 1982]). Today, the temperature difference between 0 m and 30 m water depth at the 4–2 Ma paleolocations of Site 1241 amounts to ~1.5°C.

[27] In contrast, large temperature changes occurred at the bottom of the photic zone (Figure 4a). At East Pacific Warm Pool Site 1241, the temperature record of *G. tumida* reveals a long-term decrease of 6°C during the early Pliocene with a major step between ~4.8 and ~4.0 Ma [*Steph et al.*, 2006b]. The corresponding increase in the temperature gradient between the mixed layer and the bottom of the photic zone has been interpreted as a decrease in TCD [*Steph et al.*, 2006b]. The thermocline at Site 1241 remained shallow between ~4.0 and ~3.0 Ma. The subsurface temperature changes

monitored by Mg/Ca_{G. tumida} at equatorial upwelling Site 1239 off Ecuador (Figures 1 and 4a) are very similar to those observed at Site 1241, and also point to thermocline shoaling during the early Pliocene. Since Pliocene changes in Mg/Ca temperatures and $\delta^{18}\text{O}$ recorded by *G. tumida* show approximately the same pattern at sites 1241 and 1239 (Figure 4a), we are confident that $\delta^{18}\text{O}_{G. tumida}$ predominantly reflects temperature changes at the bottom of the photic zone (although biased by a certain amount of salinity change [*Steph et al.*, 2006b]). The fact that the *G. tumida* $\delta^{18}\text{O}$ records from tropical eastern Pacific sites 847 [*Chaisson and Ravelo*, 2000; *Wara et al.*, 2005] and 851 [*Cannariato and Ravelo*, 1997] bear a striking similarity to those from sites 1239 and 1241 suggests that the early Pliocene TCD decrease in the tropical eastern Pacific between 4.8 and 4.0 Ma was a large-scale phenomenon that spread across tropical oceanic fronts (Figures 1 and 4b). The temperature increase at the bottom of the photic zone after ~3.0 Ma observed at doldrum Site 1241 (derived from Mg/Ca_{G. tumida}) points to thermocline deepening outside the EEP cold tongue region (Figure 4a), and does hence not support the hypothesis of general thermocline shoaling around 3 Ma in response to global cooling [*Fedorov et al.*, 2006].

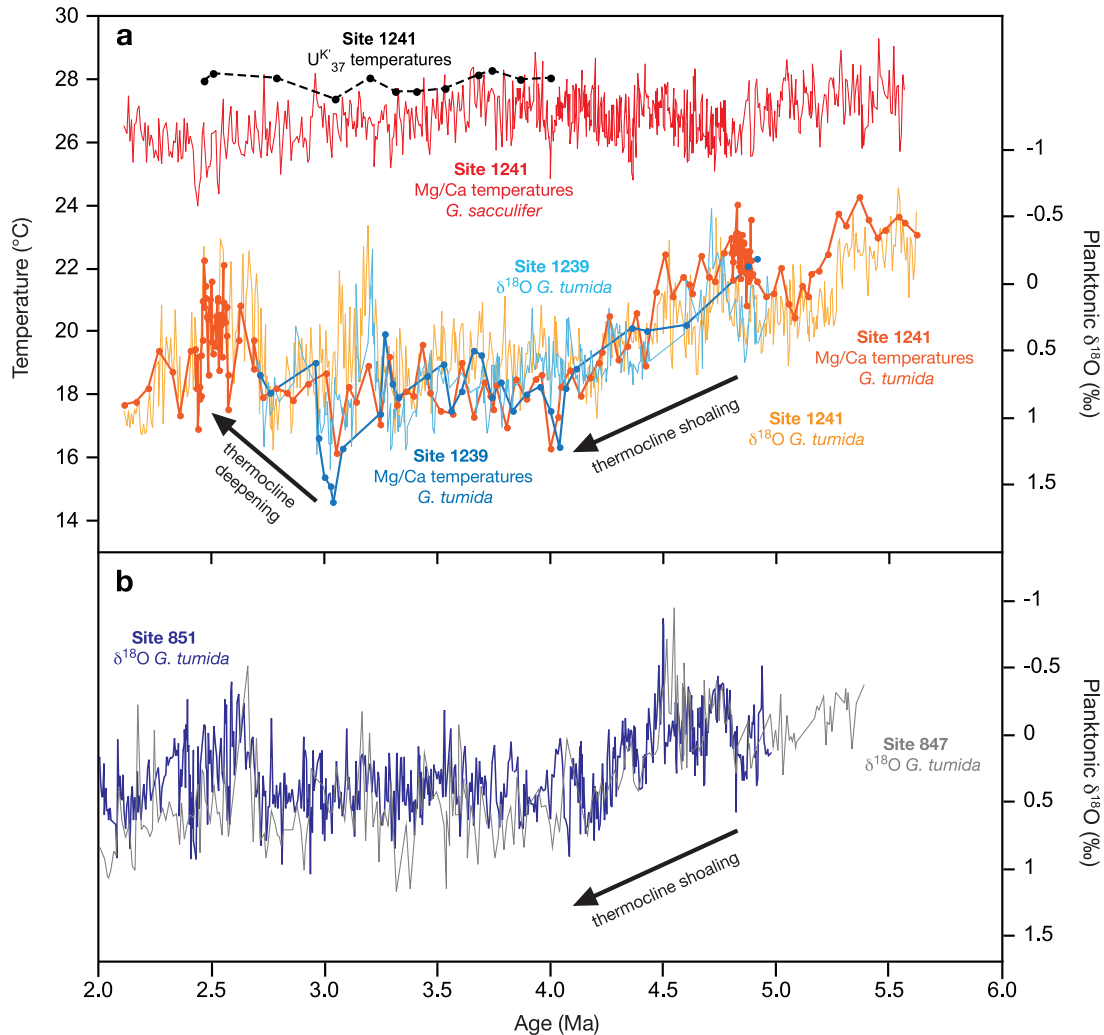


Figure 4. (a) Pliocene changes in tropical eastern Pacific upper ocean stratification. Top lines show $U_{37}^{K'}$ SSTs from East Pacific Warm Pool Site 1241 (this study, black dashed line with dots) and Mg/Ca mixed layer temperatures (*G. sacculifer*) from Site 1241 (red line) [Groeneveld *et al.*, 2006]. Bottom lines show *G. tumida* Mg/Ca temperature records (bottom of the photic zone, ~80–100 m water depth) from sites 1241 (red line with dots) [Steph *et al.*, 2006b] and 1239 (dark blue, EEP cold tongue, this study), as well as *G. tumida* $\delta^{18}O$ data from sites 1241 (orange) [Steph *et al.*, 2006b] and 1239 (light blue, this study). (b) Pliocene *G. tumida* $\delta^{18}O$ data from tropical eastern Pacific sites 851 (dark blue) [Cannariato and Ravelo, 1997] and 847 (gray) [Wara *et al.*, 2005].

4.2. Pliocene Changes in AMOC

[28] The timing of the observed regional TCD changes in the eastern tropical Pacific suggests a close link to changes in AMOC, as indicated by a comparison of benthic $\delta^{13}C$ data from tropical western Atlantic Site 925 [Bickert *et al.*, 1997; Tiedemann and Franz, 1997; Shackleton and Hall, 1997] and from Caribbean Site 1000. Specifically, the shoaling of the thermocline between 4.8 and 4.0 Ma was associated with AMOC strengthening, whereas the observed thermocline deepening at Site 1241 after 3 Ma was associated with a decrease in AMOC (Figure 5).

[29] Caribbean Site 1000, located at 916 m water depth, provides a window into the tropical Atlantic intermediate water level. Tropical Atlantic Site 925, located on the Ceara

Rise at 3041 m water depth, is situated within the modern core depth of Lower North Atlantic Deep Water (LNADW) (Figure 1). The comparison of changes in $\delta^{13}C$ at sites 925 and 1000 provides information about the relative proportion of northern component (high- $\delta^{13}C$) and southern component (low- $\delta^{13}C$) water and the interplay between Upper North Atlantic Deep Water (UNADW) and LNADW formation (Figure 5). Approximations for Pliocene $\delta^{13}C$ end-member values indicative of Southern Ocean intermediate water (Site 1236; southeast Pacific, 1323 m water depth [Tiedemann *et al.*, 2007]) and Southern Ocean deep water (Site 1237; southeast Pacific, 3212 m water depth [Tiedemann *et al.*, 2007]) are provided in Figure 5 (see arrows). Unfortunately, no Pliocene end-member values are available for North

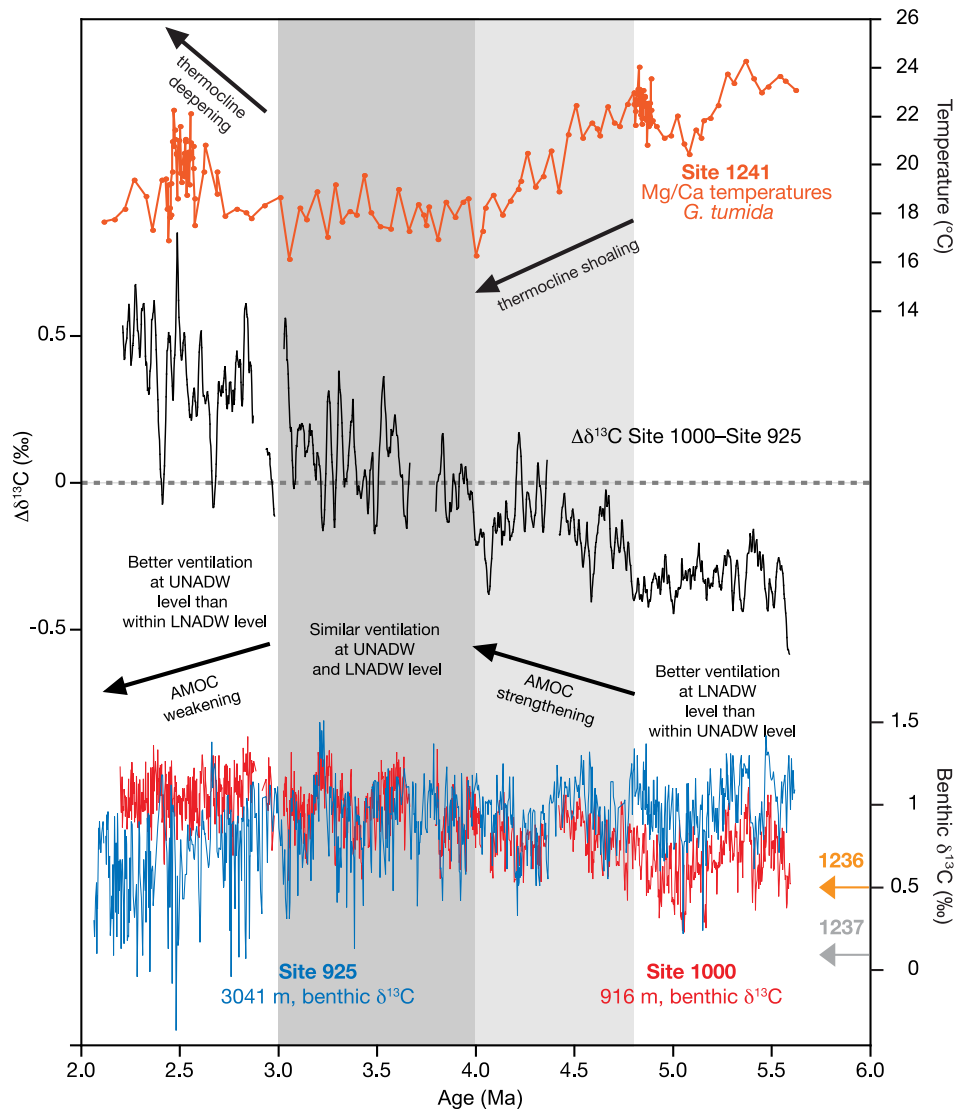


Figure 5. (top) *G. tumida* Mg/Ca temperature record from eastern Pacific Warm Pool Site 1241 (red line with dots) showing Pliocene changes in tropical eastern Pacific thermocline depth. (middle) $\Delta\delta^{13}\text{C}$ between Site 1000 (this study) and Site 925 [Bickert *et al.*, 1997; Tiedemann and Franz, 1997; Shackleton and Hall, 1997]. Before calculating the $\delta^{13}\text{C}$ difference between sites, both $\delta^{13}\text{C}$ records were evenly sampled at 2 kyr steps and smoothed using a 10-point running mean. This plot serves to clarify the timing of changes in the $\delta^{13}\text{C}$ difference between sites 1000 and 925 as mentioned in the text. Prior to 4.8 Ma, values < 0 suggest a large component of southern sourced water masses at the UNADW level (since intermediate water records from Caribbean Site 1000 and southeast Pacific Site 1236 [Tiedemann *et al.*, 2007] have similar $\delta^{13}\text{C}$ values) and weak AMOC. The decrease in $\Delta\delta^{13}\text{C}$ from ~ 4.8 Ma to ~ 4.0 Ma is marked by an increase in northern component water at the UNADW level and indicates AMOC strengthening. $\Delta\delta^{13}\text{C}$ values around 0 between 4 Ma and 3 Ma indicate a similar degree of ventilation at the UNADW and LNADW level. As $\delta^{13}\text{C}$ values at both sites are high during this interval, this points to enhanced AMOC. $\Delta\delta^{13}\text{C}$ values > 0 after ~ 3 Ma result from decreasing $\delta^{13}\text{C}$ values at LNADW Site 925. This indicates a larger component of southern sourced water masses at the LNADW level and reflects AMOC weakening, especially during harsh climate episodes. (bottom) Comparison of benthic $\delta^{13}\text{C}$ records from Caribbean Site 1000 (red, this study) and western Atlantic Site 925 (blue) [Bickert *et al.*, 1997; Tiedemann and Franz, 1997; Shackleton and Hall, 1997]. Arrows approximate average Pliocene $\delta^{13}\text{C}$ end-members of southern sourced water masses (orange arrow is for Site 1236, $21^{\circ}22'\text{S}$, $81^{\circ}26'\text{W}$, 1323 m water depth, Southern Ocean intermediate water [Tiedemann *et al.*, 2007]; gray arrow is for Site 1237, $16^{\circ}00'\text{S}$, $76^{\circ}23'\text{W}$, 3212 m water depth, Southern Ocean circumpolar deep water [Tiedemann *et al.*, 2007]).

Atlantic intermediate water masses. However, $\delta^{13}\text{C}$ values at Site 1000 higher than $\sim 0.5\text{‰}$ (average Pliocene $\delta^{13}\text{C}$ value at Southern Ocean intermediate water Site 1236) can only be explained by admixture of northern sourced (comparatively high $\delta^{13}\text{C}$) intermediate water masses. At the core depth of LNADW (Site 925), $\delta^{13}\text{C}$ values between 5.5 and 3.0 Ma were always too high to be explained by a significant contribution of southern sourced water masses. This suggests that the $\delta^{13}\text{C}$ contrast between northern and southern end-members was strong and relatively constant during the early to middle Pliocene.

[30] Our findings generally support previous studies, which documented that changes in AMOC were linked to a threshold in the closure history of the CAS during the early Pliocene and to the mid-Pliocene intensification of NHG [e.g., Keigwin, 1978; Oppo *et al.*, 1995; Haug and Tiedemann, 1998; Haug *et al.*, 2001]. Between 5.5 and 3.2 Ma, average $\delta^{13}\text{C}$ values at Site 925 were relatively high ($\sim 1\text{‰}$), indicating the continuous presence of well-ventilated LNADW (Figure 5). At Site 1000, however, $\delta^{13}\text{C}$ -depleted Southern Ocean intermediate water masses dominated before ~ 4.9 – 4.8 Ma. After 4.8 Ma, the $\delta^{13}\text{C}$ difference between sites 925 and 1000 started to decrease until benthic $\delta^{13}\text{C}$ at Site 1000 reached values identical to those at Site 925 by ~ 4.0 Ma (Figure 5). This points to a first maximum in UNADW production in the Labrador Sea. The long-term $\delta^{13}\text{C}$ increase at UNADW Site 1000 was paralleled by thermocline shoaling in the tropical eastern Pacific. The intensification of UNADW formation has been attributed to enhanced salt transfer into the high northern latitudes via the Gulf Stream in response to shoaling of the CAS [e.g., Keigwin, 1978; Haug and Tiedemann, 1998].

[31] By comparing early Pliocene changes in benthic $\delta^{13}\text{C}$ at sites 1000 and 925, we obtain basically the same results as Haug and Tiedemann [1998] and Haug *et al.* [2001], who used benthic $\delta^{13}\text{C}$ records from Caribbean Site 999 (2828 m water depth), east Atlantic ODP Site 659 (3070 m water depth) and ODP Site 849 (deep Pacific end-member). It was recently questioned, however, whether benthic $\delta^{13}\text{C}$ changes at Site 999 (which is located ~ 1000 m below the Atlantic/Caribbean sill depth) indeed reflect Pliocene changes in Atlantic intermediate water circulation [Molnar, 2008]. The significant advantage of our new $\delta^{13}\text{C}$ record from Site 1000 (916 m water depth) is that it monitors changes in water mass characteristics well above the Atlantic/Caribbean sill depth (~ 1900 m), where the exchange between Atlantic and Caribbean intermediate waters was unhampered. Although the long-term trend of $\delta^{13}\text{C}$ changes is similar at sites 999 and 1000, absolute $\delta^{13}\text{C}$ values at Site 1000 are significantly higher than those from Site 999 [Haug and Tiedemann, 1998]. This demonstrates the comparatively stronger influence of UNADW at the shallower Site 1000 (with $\delta^{13}\text{C}$ values of up to 1.1‰ ; Figure 5). Such high $\delta^{13}\text{C}$ values are not observed in Southern Ocean sourced deep and intermediate water masses [Tiedemann *et al.*, 2007].

[32] High and nearly identical benthic $\delta^{13}\text{C}$ values at sites 1000 (UNADW) and 925 (LNADW) persisted between ~ 4.0 and 3.0 Ma (Figure 5). This corroborates the general consensus of a “superconveyor” with strong UNADW and LNADW formation [e.g., Raymo *et al.*, 1996; Ravelo and

Andreasen, 2000] and coincides with the establishment and persistence of a shallow thermocline in the tropical east Pacific. Along with the first appearance of larger ice sheets on northern continents, $\delta^{13}\text{C}$ values started to decrease at Site 925, but remained high at Site 1000 (Figure 5). During harsh climate episodes, UNADW production stayed high (high $\delta^{13}\text{C}$ values at UNADW Site 1000) whereas LNADW formation was reduced [Oppo *et al.*, 1995], allowing poorly ventilated bottom waters from the Southern Ocean to penetrate to shallower water depths and farther to the north (low $\delta^{13}\text{C}$ values at LNADW Site 925). This weakening of the AMOC was paralleled by a moderate thermocline deepening in the tropical eastern Pacific (Figure 5).

4.3. Changes in Caribbean Thermocline Depth

[33] In order to assess Pliocene variations in TCD at Caribbean sites 999 and 1000, we compare Mg/Ca temperature and $\delta^{18}\text{O}$ data of the thermocline dweller *N. dutertrei* to previously published Mg/Ca temperature data of the mixed layer dweller *G. sacculifer* from Caribbean sites 999 and 1000 [Groeneveld, 2005; Groeneveld *et al.*, 2008] (Figure 6). A recent tropical Atlantic/Caribbean core top study indicates that $\delta^{18}\text{O}_{N. dutertrei} - \delta^{18}\text{O}_{G. sacculifer}$ can serve as a faithful recorder of TCD in the western Atlantic and Caribbean. Core top $\delta^{18}\text{O}_{N. dutertrei}$ and hence $\delta^{18}\text{O}_{N. dutertrei} - \delta^{18}\text{O}_{G. sacculifer}$ decreases significantly with increasing TCD, although *N. dutertrei* tends to calcify deeper in the water column if the thermocline is deep [Steph *et al.*, 2009].

[34] In this study, we use *G. sacculifer* Mg/Ca temperature records instead of $\delta^{18}\text{O}_{G. sacculifer}$, because early Pliocene mixed layer $\delta^{18}\text{O}$ changes in the Caribbean were predominantly driven by salinity [e.g., Haug *et al.*, 2001; Steph *et al.*, 2006a]. Mixed layer temperatures at both Caribbean sites show only small variations during the early Pliocene (Figure 6), whereas the Dekens *et al.* [2002] dissolution-corrected Mg/Ca temperature estimates suggest $\sim 1.5^\circ\text{C}$ higher temperatures at Site 1000 (on average 26.8°C) than at Site 999 (on average 25.3°C ; Figure 6). Without dissolution corrections (using, i.e., the Mg/Ca temperature calibration of Anand *et al.* [2003]), the temperature difference between both sites would amount to $\sim 3^\circ\text{C}$. Today, temperatures at 40–80 m water depth (estimated modern calcification depth of *G. sacculifer* in the Caribbean [Steph *et al.*, 2006a]) are $\sim 1^\circ\text{C}$ higher at Site 1000 than at Site 999 (NOCD, 2001 [Conkright *et al.*, 2002]). Yet it is possible that this temperature difference was slightly enlarged during the early Pliocene, since Site 999 was located closer to the final openings of the CAS than Site 1000 (which was probably less affected by the comparatively cool Pacific inflow as discussed by Steph *et al.* [2006a] (see Figure 1)). Accordingly, mixed layer temperatures at Pacific Site 1241 and at Caribbean Site 999 should have been similar as long as Pacific surface water entered the Caribbean via the CAS (not necessarily at Site 1000, since it was located at a greater distance from the final openings of the gateway [see Steph *et al.*, 2006a]). Indeed, the measured Mg/Ca ratios of *G. sacculifer* are similar at sites 999 and 1241. Using the Dekens *et al.* [2002] Mg/Ca temperature calibration with Pacific dissolution correction factors for Site 1241 and Atlantic dissolution correction factors for Caribbean Site

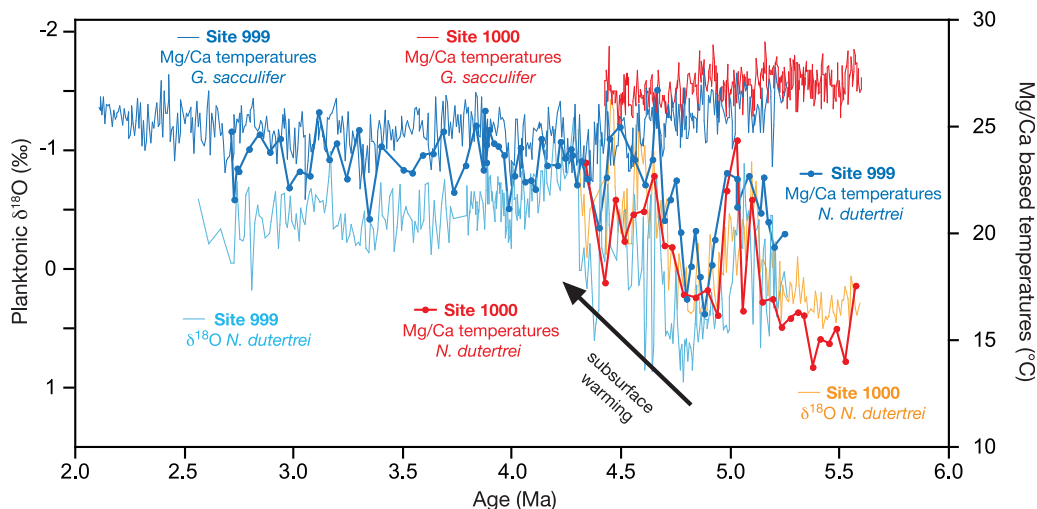


Figure 6. Changes in Caribbean upper ocean water mass signatures at ODP sites 999 and 1000 during the time interval from 5.6 to 2.1 Ma. Mg/Ca-based mixed layer temperature records (*G. sacculifer*) from sites 999 (dark blue line) [Groeneveld, 2005] and 1000 (red line) [Groeneveld et al., 2008]. The $\delta^{18}\text{O}$ records of the thermocline dweller *N. dutertrei* dextral from sites 999 (light blue line) and 1000 (orange line) and Mg/Ca temperature records of *N. dutertrei* (dextral variety) from sites 999 (thick dark blue line with dots) and 1000 (thick red line with dots).

999, however, the resulting absolute mixed layer temperature estimates are generally higher at Site 1241 than at Site 999, especially between ~ 4.6 and 2.5 Ma (compare Figures 4a and 6). This may either indicate that early Pliocene carbonate dissolution patterns were different from the modern ones (with relatively stronger carbonate dissolution in the Caribbean and/or enhanced carbonate preservation in the Pacific with respect to today), or that relatively cool water masses (not originating from the East Pacific Warm Pool; Site 1241) entered the Caribbean from the EEP cold tongue region. Yet this would imply that parts of the EEP cold tongue were already significantly cooler than the East Pacific Warm Pool during the early Pliocene (which is not supported by the alkenone SST record from EEP cold tongue Site 846 [Lawrence et al., 2006]).

[35] Since Pliocene mixed layer temperatures at Caribbean sites 999 and 1000 remained relatively constant through time, the observed increase in *N. dutertrei* Mg/Ca temperatures after ~ 4.8 Ma and the resulting decrease in the temperature gradient between mixed layer (*G. sacculifer*) and the thermocline (*N. dutertrei*), as well as the contemporaneous decrease in $\delta^{18}\text{O}_{N. dutertrei}$ (Figure 6) point to a deepening/warming of the Caribbean thermocline synchronous with thermocline shoaling in the tropical eastern Pacific [e.g., Cannariato and Ravelo, 1997; Steph et al., 2006b, chapter 4.1]. The timing of this event corresponds roughly to the restriction of Pacific–Caribbean surface water exchange after 4.7–4.6 Ma [e.g., Keigwin, 1982; Haug et al., 2001; Steph et al., 2006a].

4.4. Numerical Experiments

[36] In the ECBILT–CLIO experiments, the closure of the CAS induces an overall decrease in tropical TCD, except for the Caribbean, where the thermocline deepens (Figure 3a).

This is consistent with our Pliocene TCD reconstructions for Caribbean sites 999 and 1000 (Figure 6), and with results from previously published modeling studies [Schneider and Schmittner, 2006]. We thus interpret the Caribbean TCD increase after ~ 4.8 Ma to indicate the development of the modern Caribbean Warm Pool in response to shoaling of the CAS, when the inflow of relatively cold subsurface water from the Pacific into the Caribbean became significantly reduced [e.g., Keigwin, 1982; Haug et al., 2001; Steph et al., 2006a; Groeneveld et al., 2008]. Except for the Caribbean, the global pattern of TCD change between experiments CTL and OFF shows a very similar picture in most areas of the world ocean (Figure 3b). This result provides insight into the mechanism of thermocline shoaling: Enhanced NADW formation leads to an increase in the volume of the cold water sphere and, hence, to upward thermocline shifts in the global ocean [Huang et al., 2000; Timmermann et al., 2005]. This finding suggests that the thermocline shoaling in the tropical east Pacific during the early Pliocene was the result of a global oceanic adjustment process in response to AMOC amplification, which, in turn, was induced by substantial shoaling of the CAS. Changes in wind stress owing to AMOC intensification were unlikely to account for the thermocline shoaling in the eastern equatorial Pacific (compared to experiments CAS and OFF an eastward surface wind stress anomaly is found over the entire equatorial Pacific in CTL, which tends to *deepen* the tropical thermocline in the eastern equatorial Pacific; see auxiliary material).¹ However, the simulated trade wind intensification in the southeastern tropical Pacific leads to cooling via increased evaporation and Ekman pumping that may lead to local thermocline shoaling [cf. Timmermann et

¹Auxiliary materials are available in the HTML. doi:10.1029/2008PA001645.

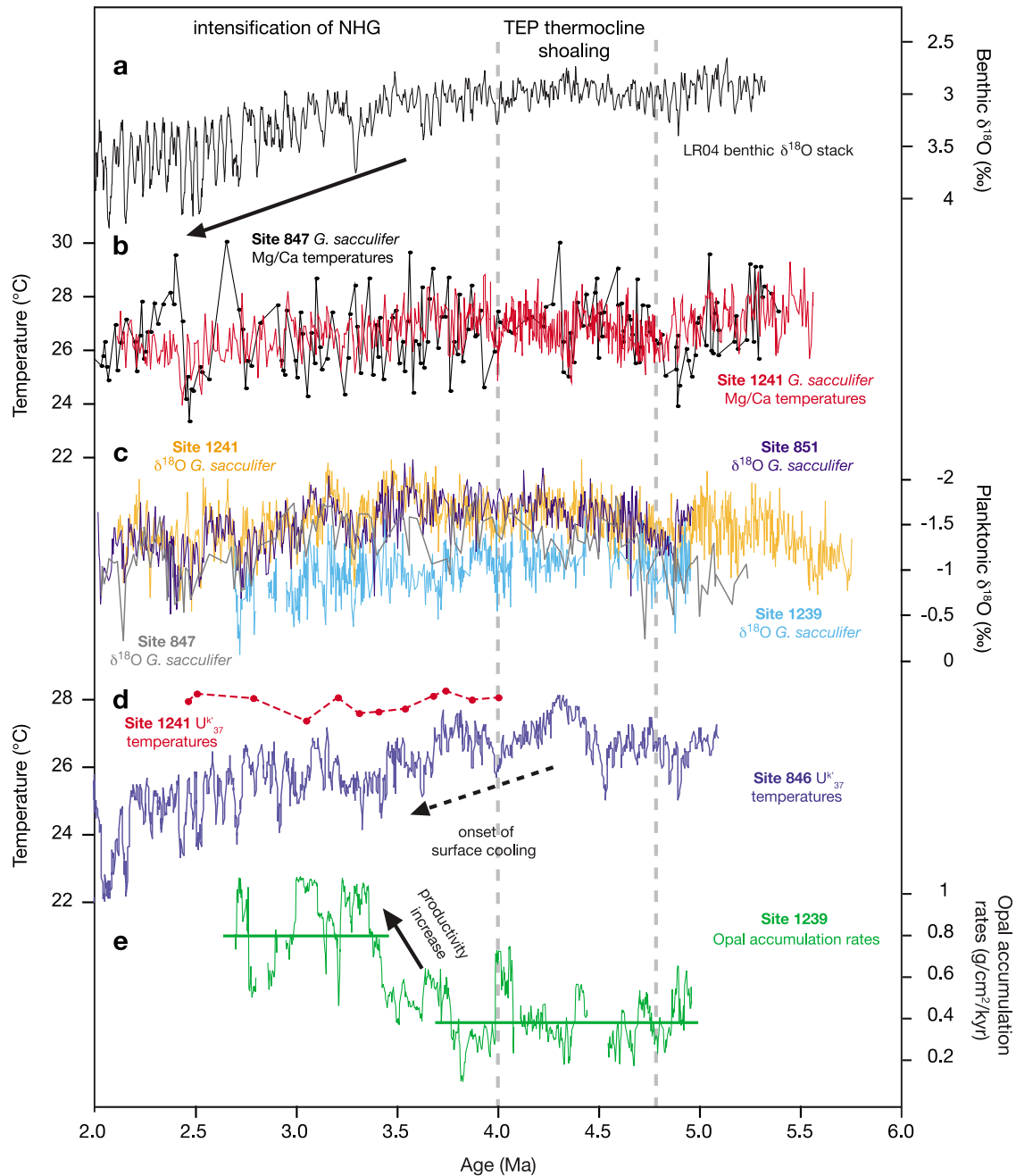


Figure 7. (a) LR04 benthic $\delta^{18}\text{O}$ stack [Lisiecki and Raymo, 2005] (black), mainly reflecting global changes in ice volume and deep water temperature. (b) Comparison of Pliocene *G. sacculifer* Mg/Ca temperatures from ODP Site 847 (black) [Wara et al., 2005] and ODP Site 1241 (red) [Groeneveld et al., 2006]. (c) Pliocene *G. sacculifer* $\delta^{18}\text{O}$ data from tropical eastern Pacific sites 1241 (orange) [Steph et al., 2006b], 851 (dark blue) [Cannariato and Ravelo, 1997], 847 (gray) [Wara et al., 2005], and 1239 (light blue, this study). (d) U_{37}^K SSTs from the Pacific doldrum region (Site 1241, red line, this study) and U_{37}^K SSTs from EEP cold tongue Site 846 (blue line) [Lawrence et al., 2006]. (e) Biogenic opal accumulation rates, Site 1239 (green line).

al., 2007b]. The early Pliocene formation of the modern Caribbean Warm Pool more than compensated for the effect of AMOC-induced thermocline shoaling on Caribbean TCD.

4.5. Development of the EEP Cold Tongue

[37] While the temperature evolution at the bottom of the photic zone in the tropical eastern Pacific was synchronous across the equator (Figure 4), a meridionally different de-

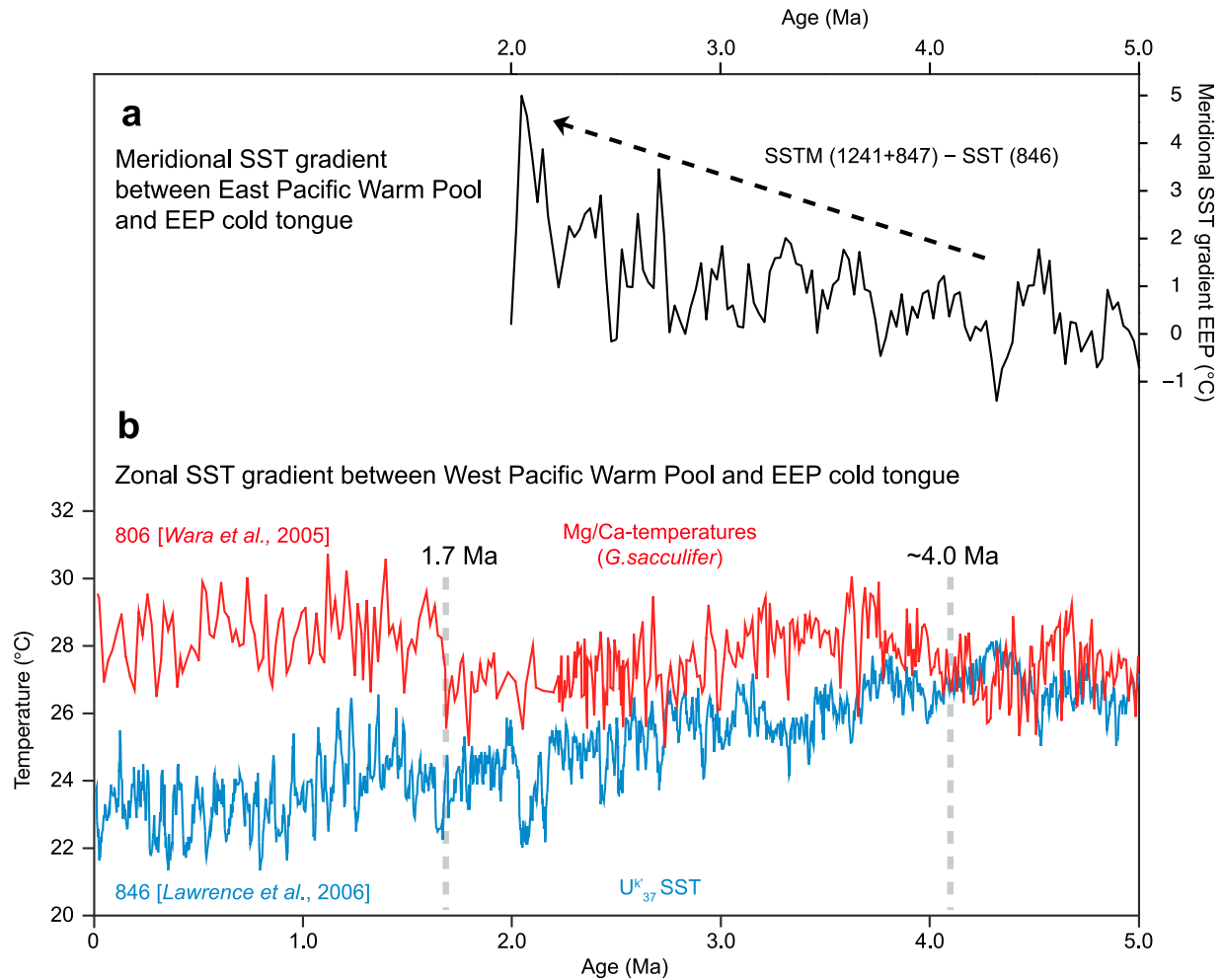


Figure 8. (a) Eastern equatorial Pacific meridional temperature gradient (°C) estimated from the difference between the mean of the Mg/Ca-based SST reconstructions from sites 1241 and 847 (northeastern equatorial Pacific [Groeneveld et al., 2006; Wara et al., 2005]) and the alkenone-based SST from site 846 (southeastern equatorial Pacific [Lawrence et al., 2006]). All SST data were filtered with a three-point running mean, and the resulting time series were interpolated onto an equidistant grid with intervals of 25,000 years using a cubic spline. The strength of the meridional SST gradient determines the position of the ITCZ in the EEP, the strength of the cross-equatorial trade winds, and hence the efficiency of equatorial upwelling [Timmermann et al., 2007a]. (b) The comparison of U_{37}^K temperatures from cold tongue Site 846 (blue) [Lawrence et al., 2006] with Mg/Ca_{G. sacculifer} derived temperatures from West Pacific Warm Pool Site 806 (red) [Wara et al., 2005; Fedorov et al., 2006] indicates that the development of the equatorial Pacific east-west SST gradient started as early as ~4.0 Ma, with a second major step occurring at 1.7 Ma as previously suggested by, e.g., Fedorov et al. [2006].

development of surface hydrography between the doldrums and the EEP cold tongue may reflect regional differences in wind stress. The similar mixed layer temperature evolution (derived from Mg/Ca_{G. sacculifer}) at doldrum Site 1241 [Groeneveld et al., 2006] and at Site 847 [Wara et al., 2005], today located at the northern edge of the EEP cold tongue, suggests that both sites were located in warm surface water outside the EEP cold tongue region during the early to middle Pliocene (Figures 1 and 7b). Absolute $\delta^{18}\text{O}$ *G. sacculifer* values and fluctuations are also similar at sites 1241, 847, and at ODP Site 851 (today located north of the modern EEP cold tongue region) [Cannariato and Ravelo,

1997; Wara et al., 2005; Steph et al., 2006b] (Figures 1 and 7c). Yet the pattern of long-term changes in $\delta^{18}\text{O}$ records displays larger deviations from their associated Mg/Ca temperature records, especially during the earliest Pliocene (Figure 7). This suggests that the $\delta^{18}\text{O}$ *G. sacculifer* signal at these sites is partly modulated by changes in mixed layer salinity.

[38] Within the EEP cold tongue region, the development of a shallow thermocline between ~4.8 and 4.0 Ma should have increased the potential of trade winds to decrease SST by initiating coastal and equatorial upwelling. Indeed, the *G. sacculifer* $\delta^{18}\text{O}$ record from equatorial upwelling Site 1239

diverges from the site 1241, 851, and 847 $\delta^{18}\text{O}_{G. \textit{sacculifer}}$ records after ~ 3.9 Ma, and more clearly after ~ 3.7 Ma, displaying relatively higher $\delta^{18}\text{O}$ values (Figure 7c). This indicates a different development of mixed layer hydrography within the EEP cold tongue region, with lower temperatures (and/or higher salinity) compared to the East Pacific Warm Pool. A more faithful recorder of the SST development within the cold tongue is the U_{37}^{K} SST record from Site 846 [Lawrence *et al.*, 2006] (Figure 7d). Today, this site is lo-

cated within the center of the EEP cold tongue, where the upwelling of cold waters is driven by Ekman divergence. The Site 846 SST estimates suggest that sea surface cooling within the EEP cold tongue region ($\sim 1^\circ\text{C}/\text{Ma}$) started between ~ 4.3 Ma and 3.6 Ma [Lawrence *et al.*, 2006]. Moderate early sea surface cooling (beginning around 4 Ma) is also observed in the upwelling area off the California margin [e.g., Dekens *et al.*, 2007; Liu *et al.*, 2008; Brierley *et al.*, 2009], but is neither reflected in the low-resolution U_{37}^{K} SST record nor in the $\text{Mg}/\text{Ca}_{G. \textit{sacculifer}}$ derived mixed layer temperature record from East Pacific Warm Pool Site 1241 (Figures 7b and 7d). Decreasing SST in the EEP cold tongue region accordingly led to strengthening of the meridional SST gradient between the northeastern (sites 847, 1241) and southeastern (Site 846) equatorial Pacific during the early Pliocene (Figure 8a). This finding is supported by our modeling results, which also indicate that intensification of the AMOC related to CAS closing resulted in lower SST in the southeastern equatorial Pacific, whereas SST in the northeastern equatorial Pacific increased (see Figure S1 in Text S1). The mechanisms involved in establishing this meridional SST gradient have been described in detail by Zhang and Delworth [2005], Timmermann *et al.* [2007b] and Xie *et al.* [2008]. They play a key role in establishing the annual cycle of SST on the equator and in modulating ENSO variability.

[39] Comparing the U_{37}^{K} SST record from EEP cold tongue Site 846 [Lawrence *et al.*, 2006] with the $\text{Mg}/\text{Ca}_{G. \textit{sacculifer}}$ temperature record from West Pacific Warm Pool Site 806 [Wara *et al.*, 2005; Fedorov *et al.*, 2006] furthermore suggests the initial development of an equatorial Pacific east-west SST gradient around 4.0 Ma (Figure 8b), consistent with early cooling observed in the EEP cold tongue region [e.g., Lawrence *et al.*, 2006; Dekens *et al.*, 2007]. In contrast, Fedorov *et al.* [2006] concluded that the transequatorial SST gradient was constantly weak during the time interval before ~ 1.7 Ma by comparing temperature records from Site 806 and tropical northeast Pacific Site 847. Yet the U_{37}^{K} SST record from EEP cold tongue Site 846 might be better suited for assessing the Pliocene development of the transequatorial temperature gradient than Site 847, because the similarity of mixed layer temperatures at Site 847 and at East Pacific Warm Pool Site 1241 (Figure 7b) indicates that

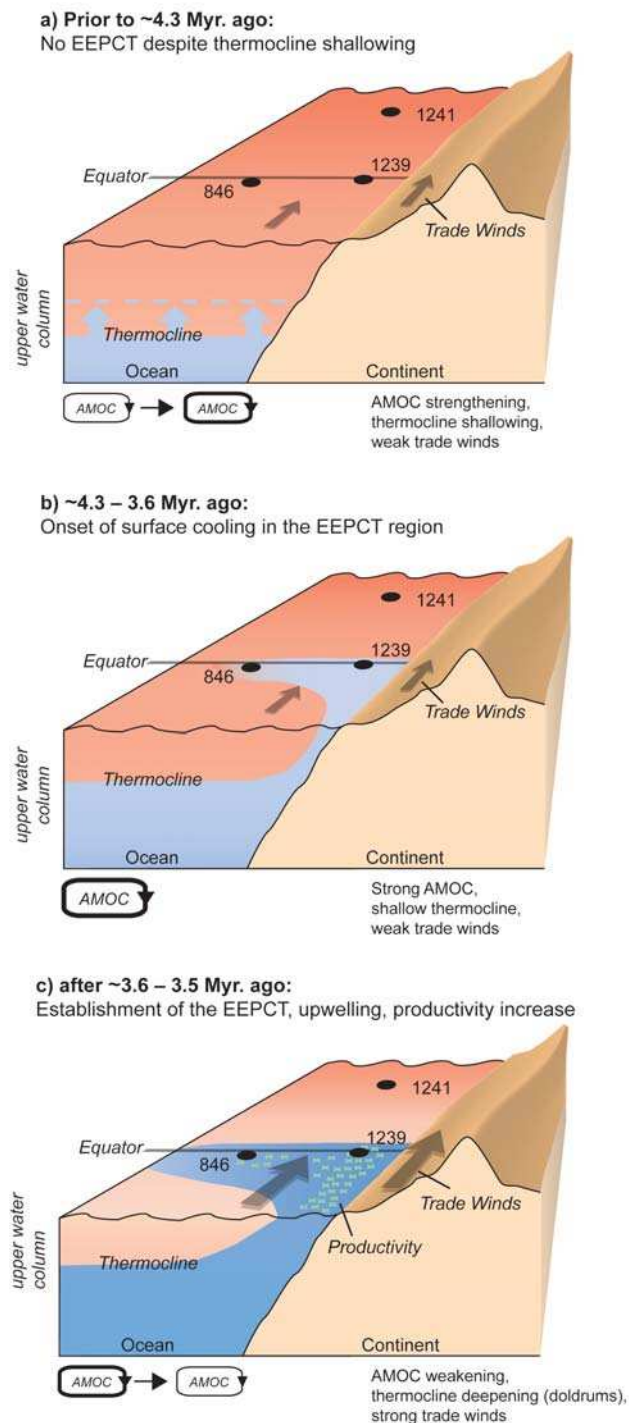


Figure 9. Schematic relationships between AMOC-induced changes in TCD and wind stress with respect to the development of the modern EEP cold tongue (EEPCT). (a) Thermocline shoaling in the tropical eastern Pacific at 4.8–4.0 Ma yielded an important precondition for the turnaround from a warm eastern equatorial Pacific to the modern EEP cold tongue state. (b) Although EEP cold tongue sea surface cooling may have started as early as ~ 4.3 –4.0 Ma ago [Lawrence *et al.*, 2006] southeast trade winds were probably too weak to significantly amplify equatorial and coastal upwelling in a warm world prior to ~ 3.6 Ma. (c) Since 3.6–3.5 Ma, changes in the tropical wind field might then have tipped the scale for an increase in upwelling and productivity parallel to the intensification of NHG [Mudelsee and Raymo, 2005].

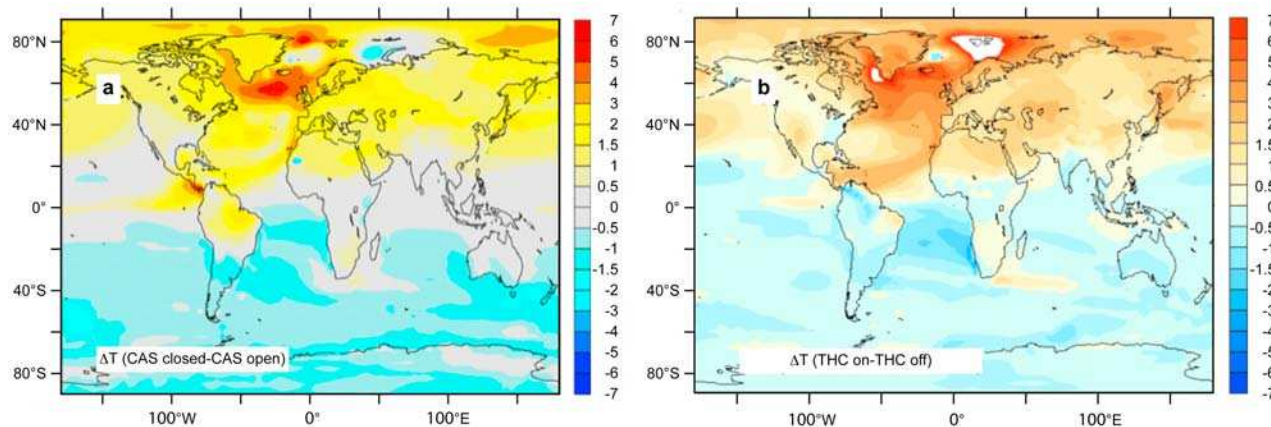


Figure 10. (a) SST response ($^{\circ}\text{C}$) to closing of the CAS (from *Lunt et al.* [2008] with kind permission of Springer Science and Business Media) as simulated by the HadCM3 coupled model. (b) SST response ($^{\circ}\text{C}$) to intensification of the AMOC as simulated by the HadCM3 model [*Timmermann et al.*, 2007b; *Dong and Sutton*, 2007].

Site 847 was probably not located in the center of the EEP cold tongue region during the early and middle Pliocene.

[40] Changes in biogenic opal accumulation rates, a proxy for biological productivity, provide additional evidence for enhanced early Pliocene upwelling in the EEP cold tongue, since this region developed as the equatorial center of diatom productivity after ~ 4.4 Ma [*Farrell et al.*, 1995]. Diatom productivity at EEP cold tongue Site 1239 increased significantly around 3.6–3.5 Ma, when opal accumulation rates doubled (Figure 7e). This change coincides with an increase in the SST gradient between doldrum Site 1241 and EEP cold tongue Site 846 (Figure 7d) and may indicate both, enhanced upwelling or an increase in nutrient concentration, which might be related to a change in advective nutrient supply. We surmise that strengthening of the pole-to-equator temperature gradient in response to the intensification of NHG enhanced trade wind strength [*Timmermann et al.*, 2004] and low-latitude upwelling since 3.6 Ma. If productivity changes are considered as additional evidence for the development of the EEP cold tongue, it occurred at least as early as 3.6–3.5 Ma.

5. Summary and Conclusions

[41] Both the early thermocline shoaling in the tropical eastern Pacific (4.8–4.0 Ma) and the early start of EEP cold tongue cooling (between ~ 4.3 Ma and 3.6 Ma) [e.g., *Lawrence et al.*, 2006; *Dekens et al.*, 2007] suggest a chain of forcing mechanisms for the development of the modern EEP cold tongue, which is different from the well-cited hypothesis that this Pliocene climate switch was predominantly linked to the major intensification of NHG (after ~ 3.0 Ma) [e.g., *Wara et al.*, 2005; *Fedorov et al.*, 2006]. Instead, the timing of these events suggests a close link to the gradual closure of the CAS, which reached a critical threshold during the earliest Pliocene, leading to the development of the modern Atlantic-Pacific salinity contrast and to the amplification of AMOC [e.g., *Keigwin*, 1982; *Haug and Tiedemann*, 1998; *Haug et al.*, 2001; *Steph et al.*, 2006a].

[42] Although the impact of the gradual CAS closure on global climate change has recently been questioned [*Molnar*, 2008], our study brings the CAS back into play by providing for the first time a consistent link between the observed decrease in tropical east Pacific TCD and an increase in the strength of the AMOC during the early Pliocene (4.8–4.0 Ma) that was triggered by a threshold in the closure history of the CAS (Figure 9). Our new Caribbean proxy data also suggests that this threshold in the CAS closure led to the formation of the modern Caribbean Warm Pool (starting at ~ 4.8 Ma), which more than compensated for AMOC-induced shoaling of the Caribbean thermocline. In contrast to previous studies, we identify changes in AMOC as a potential forcing mechanism, which consistently explains the Pliocene long-term evolution of tropical east Pacific TCD as well as the early onset of sea surface cooling in the EEP cold tongue [e.g., *Lawrence et al.*, 2006; *Dekens et al.*, 2007] and the development of a meridional SST gradient in the EEP during the early Pliocene (Figure 9).

[43] Further support for our main conclusions comes from a recent modeling study by *Lunt et al.* [2008]. Using the HadCM3 model, these authors find that closure of the CAS leads to strengthening of the AMOC as well as to warming of the Northern Hemisphere and cooling of the Southern Hemisphere (Figure 10a). This SST response to CAS closure is very similar to the SST response of the HadCM3 model to an intensification of the AMOC [*Timmermann et al.*, 2007b] (Figure 10b) and to the ECBILT-CLIO SST response to CAS closing (see auxiliary material). The enhancement of the EEP cold tongue results from a northward shift of the ITCZ and an associated southeasterly trade wind intensification south of the equator, while the wind-evaporation-SST feedback helps to maintain this feature. Summarizing, independent modeling and paleo-proxy evidence suggests that the CAS played a key role in determining the strength of the AMOC, the position of the

ITCZ, the strength of the meridional SST gradient in the EEP and the existence of the EEP cold tongue.

[44] The observed increase in biogenic productivity and upwelling within the EEP cold tongue after 3.6–3.5 Ma likely resulted from enhanced trade wind strength due to strengthening of the pole-to-equator temperature gradient in response to the intensification of NHG (Figure 9). Yet the thermocline deepening at doldrum Site 1241 after 3.0 Ma was presumably linked to AMOC weakening in response to the intensification of NHG. This contradicts the hypothesis that cooling of the deep ocean after 3.0 Ma led to a global decrease in tropical TCD.

[45] A recent analysis of IPCC model results examining the next 100 years indicates a thermodynamically driven weakening of the Walker circulation in response to global warming, possibly favoring El Niño-like climate conditions [Vecchi and Soden, 2007]. Our results further suggest changes in AMOC as an important factor for the assessment of future changes in tropical climate dynamics. If global

warming led to a reduction in both AMOC strength and trade wind intensity, the consequent increase in TCD would support the disappearance of the EEP cold tongue. Whether this mechanism may be adopted to assess future changes in ENSO variability remains to be shown.

[46] **Acknowledgments.** We thank A. Schmittner, F. Lamy, L. Reuning, and A. Sturm for discussions and criticism and D. Garbe-Schönberg, L. Haxhijaj, S. Koch, U. Nielsen, and A. Jesužek for technical assistance. We also thank the Associate Editor (David Lea) and three anonymous reviewers for their helpful comments. This research used samples and data provided by the Ocean Drilling Program, which is sponsored by the U.S. National Science Foundation and participating countries under management of Joint Oceanographic Institutions. Funding for this research was provided by the Deutsche Forschungsgemeinschaft (DFG) through projects Ti 240/7, Ti 240/12 (being part of the DFG Research Unit, FOR 451: Impact of Gateways on Ocean Circulation, Climate, and Evolution at Kiel University), and Ti 240/17 and through the DFG Research Center/Excellence Cluster “The Ocean in the Earth System” at the University of Bremen. A. Timmermann is supported by the Japan Agency for Marine-Earth Science and Technology through its sponsorship of the International Pacific Research Center.

References

- Anand, P., H. Elderfield, and M. H. Conte (2003), Calibration of Mg/Ca thermometry in planktonic foraminifera from a sediment trap time series, *Paleoceanography*, *18*(2), 1050, doi:10.1029/2002PA000846.
- Barker, S., M. Greaves, and H. Elderfield (2003), A study of cleaning procedures used for foraminiferal Mg/Ca paleothermometry, *Geochem. Geophys. Geosyst.*, *4*(9), 8407, doi:10.1029/2003GC000559.
- Bickert, T., W. B. Curry, and G. Wefer (1997), Late Pliocene to Holocene (2.6–0 Ma) western equatorial Atlantic deep-water circulation: Inferences from benthic stable isotopes, *Proc. Ocean Drill. Program Sci. Results*, *154*, 239–254.
- Brierley, C. M., A. V. Fedorov, Z. Liu, T. D. Herbert, K. T. Lawrence, and J. P. LaRiviere (2009), Greatly expanded tropical warm pool and weakened Hadley Circulation in the early Pliocene, *Science*, *323*, 1714–1718, doi:10.1126/science.1167625.
- Cannariato, K. G., and A. C. Ravelo (1997), Pliocene-Pleistocene evolution of eastern tropical Pacific surface water circulation and thermocline depth, *Paleoceanography*, *12*, 805–820, doi:10.1029/97PA02514.
- Chaisson, W. P., and A. C. Ravelo (2000), Pliocene development of the east-west hydrographic gradient in the equatorial Pacific, *Paleoceanography*, *15*, 497–505, doi:10.1029/1999PA000442.
- Conkright, M. E., R. A. Locarnini, H. E. Garcia, T. D. O'Brien, T. P. Boyer, C. Stephens, and J. I. Antonov (2002), World Ocean Atlas 2001: Objective analyses, data statistics, and figures—CD-ROM documentation, *Internal Rep. 17*, 17 pp., Nat. Oceanogr. Data Cent., Silver Spring, Md.
- Conte, M. H., M.-A. Sicre, C. Rühlemann, J. C. Weber, S. Schulte, D. Schulz-Bull, and T. Blanz (2006), Global temperature calibration of the alkenone unsaturation index (U_{37}^K) in surface waters and comparison with surface sediments, *Geochem. Geophys. Geosyst.*, *7*, Q02005, doi:10.1029/2005GC001054.
- Dekens, P. S., D. W. Lea, D. K. Pak, and H. J. Spero (2002), Core top calibration of Mg/Ca in tropical foraminifera: Refining paleotemperature estimation, *Geochem. Geophys. Geosyst.*, *3*(4), 1022, doi:10.1029/2001GC000200.
- Dekens, P. S., A. C. Ravelo, and M. D. McCarthy (2007), Warm upwelling regions in the Pliocene warm period, *Paleoceanography*, *22*, PA3211, doi:10.1029/2006PA001394.
- Dong, B., and R. Sutton (2007), Enhancement of ENSO variability by a weakened Atlantic thermohaline circulation in a coupled GCM, *J. Clim.*, *20*, 4920–4939, doi:10.1175/JCLI4284.1.
- Dowsett, H. J., J. Barron, R. Z. Poore, R. S. Thompson, T. M. Cronin, S. E. Ishman, and D. A. Willard (1999), Middle Pliocene paleoenvironmental reconstruction: PRISM2, *U.S. Geol. Surv. Open File Rep.*, 99-535, 13 pp.
- DeMaster, D. J. (1981), Measuring biogenic silica in marine sediments and suspended matter, in *Marine Particles: Analysis and Characterization*, *Geophys. Monogr. Ser.*, vol. 63, edited by D. C. Hurd and D. W. Spenser, pp. 363–368, AGU, Washington, D. C.
- Fairbanks, R. G., M. Sverdlow, R. Free, P. H. Wiebe, and A. W. H. Bé (1982), Vertical distribution and isotopic fractionation of living planktonic foraminifera from the Panama Basin, *Nature*, *298*, 841–844.
- Farrell, J. W., I. Raffi, T. R. Janecek, D. W. Murray, M. Levitan, K. A. Dadey, K. C. Emeis, M. Lyle, J. A. Flores, and S. Hovan (1995), Late Neogene sedimentation patterns in the eastern equatorial Pacific Ocean, *Proc. Ocean Drill. Program Sci. Results*, *138*, 717–756.
- Fedorov, A. V., P. S. Dekens, M. McCarthy, A. C. Ravelo, P. B. deMenocal, M. Barreiro, R. C. Pacanowski, and S. G. Philander (2006), The Pliocene paradox (mechanisms for a permanent El Niño), *Science*, *312*, 1485–1489, doi:10.1126/science.1122666.
- Foster, G. L., O. Seki, R. D. Pancost, and D. N. Schmidt (2009), pCO_2 and climate: Evidence from boron based proxies of pH and pCO_2 , *Geochim. Cosmochim. Acta*, *73*(13), suppl. 1, A391.
- Goosse, H., and T. Fichefet (1999), Importance of ice-ocean interactions for the global ocean circulation: A model study, *J. Geophys. Res.*, *104*, 23,337–23,355, doi:10.1029/1999JC900215.
- Groeneveld, J. (2005), Effect of the Pliocene closure of the Panamanian Gateway on Caribbean and East Pacific sea surface temperatures and salinities by applying combined Mg/Ca and $\delta^{18}O$ measurements (5.6–2.2 Ma), Ph.D. thesis, 161 pp., Univ. of Kiel, Kiel, Germany.
- Groeneveld, J., S. Steph, R. Tiedemann, D. Garbe-Schönberg, D. Nürnberg, and A. Sturm (2006), Pliocene mixed-layer oceanography for site 1241, using combined Mg/Ca and $\delta^{18}O$ analyses of *Globigerinoides sacculifer*, *Proc. Ocean Drill. Program Sci. Results*, *202*, 1–27, doi:10.2973/odp.proc.sr.202.209.
- Groeneveld, J., D. Nürnberg, R. Tiedemann, G.-J. Reichert, S. Steph, L. Reuning, D. Crudeli, and P. Mason (2008), Foraminiferal Mg/Ca increase in the Caribbean during the Pliocene: Western Atlantic Warm Pool formation, salinity influence, or diagenetic overprint?, *Geochem. Geophys. Geosyst.*, *9*(1), Q01P23, doi:10.1029/2006GC001564.
- Haug, G. H., and R. Tiedemann (1998), Effect of the formation of the Isthmus of Panama on Atlantic Ocean thermohaline circulation, *Nature*, *393*, 673–676, doi:10.1038/31447.
- Haug, G. H., R. Tiedemann, R. Zahn, and A. C. Ravelo (2001), Role of Panama uplift on oceanic freshwater balance, *Geology*, *29*, 207–210, doi:10.1130/0091-7613(2001)029<0207:ROPUOO>2.0.CO;2.
- Huang, R. X., M. A. Cane, N. Naik, and P. Goodman (2000), Global adjustment of the thermocline in response to deepwater formation, *Geophys. Res. Lett.*, *27*, 759–762, doi:10.1029/1999GL002365.
- Jansen, E., et al. (2007), Palaeoclimate, in *Climate Change 2007: The Physical Science Basis: Working Group I Contribution to the Fourth Assessment Report of the Intergovernmental Panel on Climate Change*, edited by S. Solomon et al., pp. 433–497, Cambridge Univ. Press, New York.
- Keigwin, L. D. (1978), Pliocene closing of the Isthmus of Panama, based on biostratigraphic

- evidence from nearby Pacific Ocean and Caribbean Sea cores, *Geology*, **6**, 630–634, doi:10.1130/0091-7613(1978)6<630:PCOTIO>2.0.CO;2.
- Keigwin, L. D. (1982), Isotopic paleoceanography of the Caribbean and East Pacific: Role of Panama uplift in late Neogene time, *Science*, **217**, 350–352, doi:10.1126/science.217.4557.350.
- Klocker, A., M. Prange, and M. Schulz (2005), Testing the influence of the Central American Seaway on orbitally forced Northern Hemisphere glaciation, *Geophys. Res. Lett.*, **32**, L03703, doi:10.1029/2004GL021564.
- Kroopnick, P. M. (1985), The distribution of ^{13}C in the world oceans, *Deep Sea Res., Part A*, **32**, 57–84, doi:10.1016/0198-0149(85)90017-2.
- Lawrence, K. T., Z. Liu, and T. D. Herbert (2006), Evolution of the eastern tropical Pacific through Plio-Pleistocene glaciation, *Science*, **312**, 79–83, doi:10.1126/science.1120395.
- Lisiecki, L. E., and M. E. Raymo (2005), A Pliocene-Pleistocene stack of 57 globally distributed benthic $\delta^{18}\text{O}$ records, *Paleoceanography*, **20**, PA1003, doi:10.1029/2004PA001071.
- Liu, Z., M. A. Altabet, and T. D. Herbert (2008), Plio-Pleistocene denitrification in the eastern tropical North Pacific: Intensification at 2.1 Ma, *Geochem. Geophys. Geosyst.*, **9**, Q11006, doi:10.1029/2008GC002044.
- Lunt, D. J., P. J. Valdes, A. Haywood, and I. C. Rutt (2008), Closure of the Panama Seaway during the Pliocene: Implications for climate and Northern Hemisphere glaciation, *Clim. Dyn.*, **30**, 1–18, doi:10.1007/s00382-007-0265-6.
- Maier-Reimer, E., U. Mikolajewicz, and T. Crowley (1990), Ocean general circulation model sensitivity experiments with an open Central American Isthmus, *Paleoceanography*, **5**, 349–360, doi:10.1029/PA005i003p00349.
- Marlow, J. R., C. B. Lange, G. Wefer, and A. Rosell-Melé (2000), Upwelling intensification as part of the Pliocene-Pleistocene climate transition, *Science*, **290**, 2288–2291.
- McCorkle, D. C., and L. D. Keigwin (1994), Depth profiles of $\delta^{13}\text{C}$ in bottom water and core top *C. wuellerstorfi* on the Ontong Java Plateau and Emperor seamounts, *Paleoceanography*, **9**, 197–208, doi:10.1029/93PA03271.
- Mix, A. C., et al. (2003), *Proceedings of the Ocean Drilling Program: Initial Reports*, vol. 202, Ocean Drill. Program, College Station, Tex.
- Molnar, P. (2008), Closing of the Central American Seaway and the Ice Age: A critical review, *Paleoceanography*, **23**, PA2201, doi:10.1029/2007PA001574.
- Molnar, P., and M. A. Cane (2002), El Niño's tropical climate and teleconnections as a blueprint for pre-Ice Age climates, *Paleoceanography*, **17**(2), 1021, doi:10.1029/2001PA000663.
- Mudelsee, M., and M. E. Raymo (2005), Slow dynamics of the Northern Hemisphere glaciation, *Paleoceanography*, **20**, PA4022, doi:10.1029/2005PA001153.
- Müller, P. J., and R. Schneider (1993), An automated leaching method for the determination of opal in sediments and particulate matter, *Deep Sea Res., Part I*, **40**, 425–444, doi:10.1016/0967-0637(93)90140-X.
- Oppo, D. W., M. E. Raymo, G. P. Lohmann, A. C. Mix, J. D. Wright, and W. L. Prell (1995), A $\delta^{13}\text{C}$ record of upper North Atlantic deep water during the past 2.6 million years, *Paleoceanography*, **10**, 373–394, doi:10.1029/95PA00332.
- Opsteegh, J. D., R. J. Haarsma, F. M. Selten, and A. Kattenberg (1998), ECBILT: A dynamic alternative to mixed boundary conditions in ocean models, *Tellus, Ser. A*, **50**, 348–367.
- Prange, M., and M. Schulz (2004), A coastal upwelling seesaw in the Atlantic Ocean as a result of the closure of the Central American Seaway, *Geophys. Res. Lett.*, **31**, L17207, doi:10.1029/2004GL020073.
- Ravelo, A. C., and D. H. Andreasen (1999), Using planktonic foraminifera as monitors of the tropical surface ocean, in *Reconstructing Ocean History—A Window Into the Future*, edited by F. Abrantes and A. Mix, pp. 217–244, Plenum, New York.
- Ravelo, A. C., and D. H. Andreasen (2000), Enhanced circulation during a warm period, *Geophys. Res. Lett.*, **27**, 1001–1004, doi:10.1029/1999GL007000.
- Ravelo, A. C., and R. G. Fairbanks (1992), Oxygen isotopic composition of multiple species of planktonic foraminifera: Recorders of the modern photic zone temperature gradient, *Paleoceanography*, **7**, 815–832, doi:10.1029/92PA02092.
- Ravelo, A. C., D. H. Andreasen, M. Lyle, A. O. Lyle, and M. W. Wara (2004), Regional climate shifts caused by gradual global cooling in the Pliocene epoch, *Nature*, **429**, 263–267, doi:10.1038/nature02567.
- Raymo, M. E., B. Grant, M. Horowitz, and G. H. Rau (1996), Mid-Pliocene warmth: Stronger greenhouse and stronger conveyor, *Mar. Micropaleontol.*, **27**, 313–326, doi:10.1016/0377-8398(95)00048-8.
- Schneider, B., and A. Schmittner (2006), Simulating the impact of the Panamanian Seaway closure on ocean circulation, marine productivity and nutrient cycling, *Earth Planet. Sci. Lett.*, **246**, 367–380, doi:10.1016/j.epsl.2006.04.028.
- Shackleton, N. J., and M. A. Hall (1997), The late Miocene stable isotope record: Site 926, *Proc. Ocean Drill. Program Sci. Results*, **154**, 367–373.
- Sigurdsson, H., et al. (1997), *Proceedings of the Ocean Drilling Program: Initial Reports*, vol. 165, Ocean Drill. Program, College Station, Tex.
- Steph, S., R. Tiedemann, M. Prange, J. Groeneveld, D. Nürnberg, L. Reuning, M. Schulz, and G. H. Haug (2006a), Changes in Caribbean surface hydrography during the Pliocene shoaling of the Central American Seaway, *Paleoceanography*, **21**, PA4221, doi:10.1029/2004PA001092.
- Steph, S., R. Tiedemann, J. Groeneveld, A. Sturm, and D. Nürnberg (2006b), Pliocene changes in tropical East Pacific upper ocean stratification: Response to tropical gateways?, *Proc. Ocean Drill. Program Sci. Results*, **202**, 1–51, doi:10.2973/odp.proc.sr.202.211.2006.
- Steph, S., M. Regenberg, R. Tiedemann, S. Mulitza, and D. Nürnberg (2009), Stable isotopes of planktonic foraminifera from tropical Atlantic/Caribbean core-tops: Implications for reconstructing upper ocean stratification, *Mar. Micropaleontol.*, **71**, 1–19, doi:10.1016/j.micropaleontol.2008.12.004.
- Tiedemann, R., and S. O. Franz (1997), Deep-water circulation, chemistry, and terrigenous sediment supply in the equatorial Atlantic during the Pliocene, 3.3–2.6 Ma and 5–4.5 Ma, *Proc. Ocean Drill. Program Sci. Results*, **154**, 299–318.
- Tiedemann, R., A. Sturm, S. Steph, S. P. Lund, and J. S. Stoner (2007), Astronomically calibrated time scales from 6–2.5 Ma and benthic isotope stratigraphies of sites 1236, 1237, 1239 and 1241, *Proc. Ocean Drill. Program Sci. Results*, **202**, 1–69, doi:10.2973/odp.proc.sr.202.210.2007.
- Timmermann, A., F. B. Justino, F.-F. Jin, and H. Goosse (2004), Surface temperature control in the North and tropical Pacific during the Last Glacial Maximum, *Clim. Dyn.*, **23**, 353–370, doi:10.1007/s00382-004-0434-9.
- Timmermann, A., S.-I. An, U. Krebs, and H. Goosse (2005), ENSO suppression due to weakening of the North Atlantic thermohaline circulation, *J. Clim.*, **18**, 3122–3139, doi:10.1175/JCLI3495.1.
- Timmermann, A., S. J. Lorenz, S.-I. An, A. Clement, and S.-P. Xie (2007a), The effect of orbital forcing on the mean climate and variability of the tropical Pacific, *J. Clim.*, **20**, 4147–4159, doi:10.1175/JCLI4240.1.
- Timmermann, A., et al. (2007b), The influence of a weakening of the Atlantic meridional overturning circulation on ENSO, *J. Clim.*, **20**, 4899–4919, doi:10.1175/JCLI4283.1.
- Vecchi, G. A., and B. J. Soden (2007), Global warming and the weakening of the tropical circulation, *J. Clim.*, **20**, 4316–4340, doi:10.1175/JCLI4258.1.
- Wara, M. W., A. C. Ravelo, and M. L. Delaney (2005), Permanent El Niño-like conditions during the Pliocene warm period, *Science*, **309**, 758–761, doi:10.1126/science.1112596.
- Xie, S.-P., Y. Okumura, T. Miyama, and A. Timmermann (2008), Influences of Atlantic climate change on the tropical Pacific via the Central American Isthmus, *J. Clim.*, **21**, 3914–3928, doi:10.1175/2008JCLI2231.1.
- Zahn, R., K. Winn, and M. Samthein (1986), Benthic foraminiferal $\delta^{13}\text{C}$ and accumulation rates of organic carbon: *Uvigerina peregrina* group and *Cibicides wuellerstorfi*, *Paleoceanography*, **1**, 27–42, doi:10.1029/PA001i001p00027.
- Zhang, R., and T. Delworth (2005), Simulated tropical response to a substantial weakening of the Atlantic thermohaline circulation, *J. Clim.*, **18**, 1853–1860, doi:10.1175/JCLI3460.1.

J. Groeneveld, M. Prange, and M. Schulz, Department of Geosciences, University of Bremen, D-28359 Bremen, Germany.

G. H. Haug, Geological Institute, Department of Earth Sciences, ETH Zurich, CH-8092 Zurich, Switzerland.

D. Nürnberg, Leibniz Institute of Marine Sciences at University of Kiel (IFM-GEOMAR), D-24148 Kiel, Germany.

C. Rühlemann, Bundesanstalt für Geowissenschaften und Rohstoffe, D-30655 Hannover, Germany.

C. Saukel and R. Tiedemann, Alfred Wegener Institute for Polar and Marine Research, D-27568 Bremerhaven, Germany.

S. Steph, DFG-Leibniz Center for Surface Process and Climate Studies, Institute for Geosciences, Potsdam University, D-14476 Potsdam, Germany. (ssteph@whoi.edu)

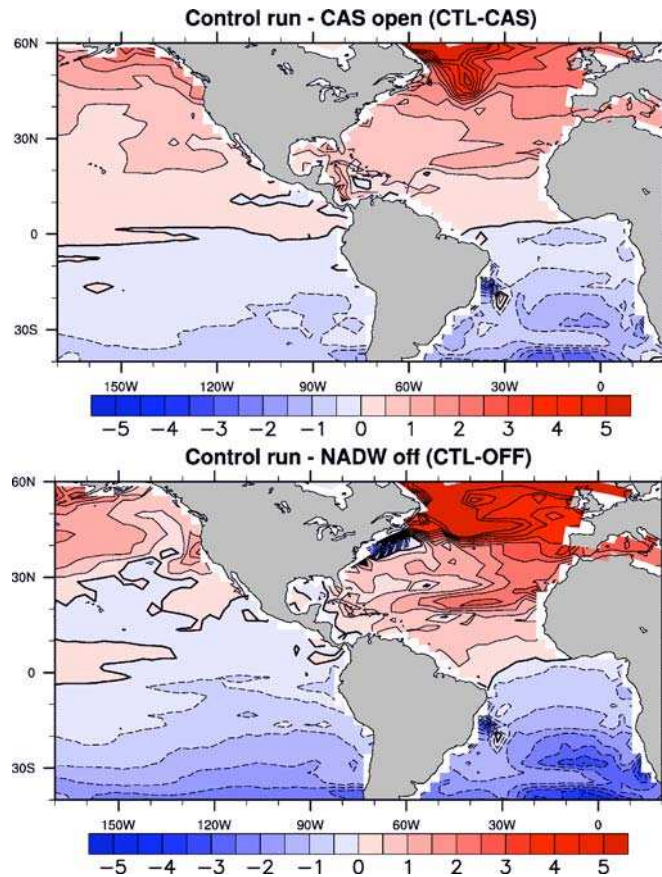
A. Timmermann, IPRC, SOEST, University of Hawai'i at Mānoa, Honolulu, HI 96822, USA.

Supplementary information

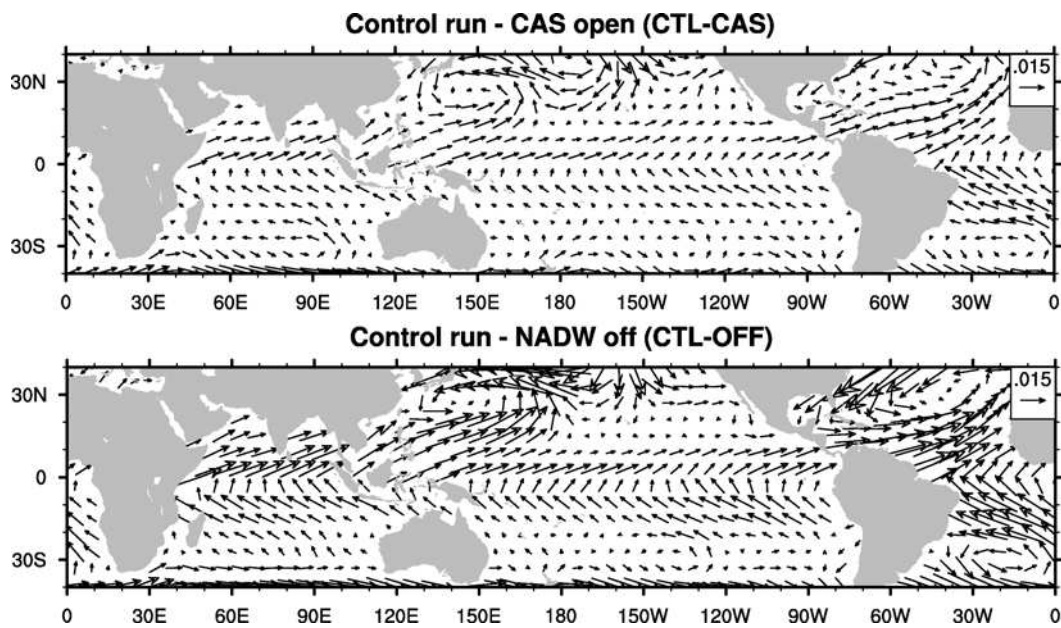
Assessing the influence of wind-stress changes on Pacific thermocline depth

Cooling of the North Atlantic induced by a weakening of the AMOC does not only affect the atmospheric circulation in the North Atlantic realm. *Zhang and Delworth* [2005] identified an “atmospheric bridge” that conveys a cooling signal from the tropical North Atlantic to the Pacific via the Central American region. As a result, trade winds intensify over the northeastern tropical Pacific and a southward surface wind anomaly is induced across the equator. In addition, strong cooling over the North Atlantic may excite a large-scale stationary wave pattern, resulting in an anomalous cyclonic surface wind over the extratropical North Pacific [*Zhang and Delworth*, 2005]. Hence, changes in surface wind-stress cannot be ruled out *a priori* as a factor in modifying the Pacific TCD. In the following, however, we demonstrate that wind-stress effects do *not* account for the changes in eastern equatorial Pacific TCD found in the ECBILT-CLIO model experiments, supporting our explanation of an internal oceanic adjustment process [*Timmermann et al.*, 2005] that determines the depth of the eastern Pacific tropical thermocline.

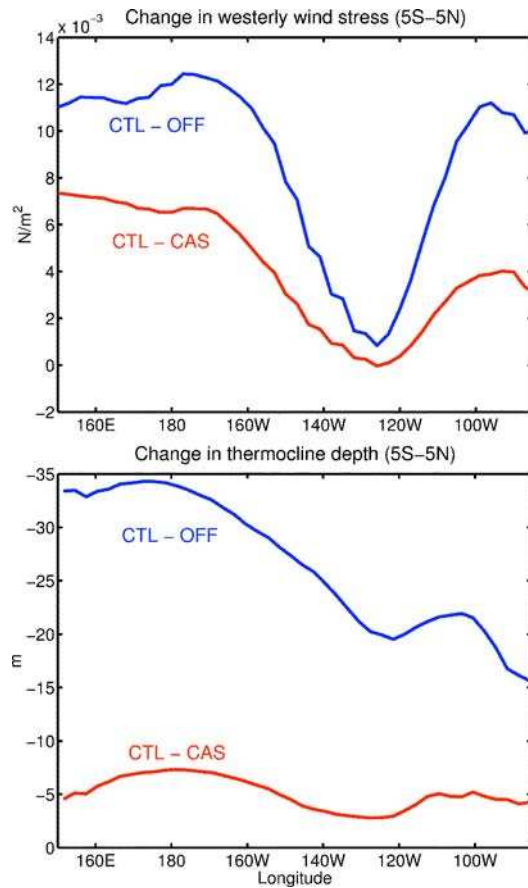
Suppl.-Fig. 1 shows differences in sea-surface temperature for CTL minus CAS (top) and CTL minus OFF (bottom). The warming of the North Atlantic realm in response to AMOC intensification is clearly visible in both cases. As a consequence, ECBILT-CLIO simulates both the tropical atmospheric bridge and the extratropical teleconnection between the Atlantic and Pacific oceans in both experiments CAS and OFF (note that the sign of changes is opposite as compared to *Zhang and Delworth* [2005], since we consider here the effect of AMOC *strengthening* rather than weakening). The warming of the North Atlantic in experiment CTL relative to CAS and OFF results in a weakening of the trade winds over the northeastern tropical Pacific with corresponding changes in surface wind-stress (Suppl.-Fig. 2). Suppl.-Fig. 3 displays the changes in wind stress over the equatorial Pacific. Compared to experiments CAS and OFF an eastward surface stress-anomaly is found in the control run over the entire equatorial Pacific. This eastward anomaly tends to *deepen* the tropical thermocline in the eastern Pacific. Hence, wind-stress anomalies tend to work against the internal thermocline adjustment mechanism and cannot account for the eastern equatorial Pacific thermocline shoaling in response to AMOC intensification. We further note that the simulated TCD increase in the Pacific north of $\sim 20^\circ\text{N}$ (Fig. 2) is attributable to extratropical changes in surface wind-stress and the associated Ekman pumping.



Suppl.-Fig. 1. Differences in annual-mean sea-surface temperature ($^{\circ}\text{C}$) between the ECBILT-CLIO present-day control run CTL and (top) experiment CAS and (bottom) experiment OFF.



Suppl.-Fig. 2. Differences in annual-mean surface wind-stress (N m^{-2}) between the ECBILT-CLIO present-day control run CTL and (top) experiment CAS and (bottom) experiment OFF.



Suppl.-Fig. 3. Eastward component of surface wind-stress anomalies over the equatorial Pacific (top) and tropical Pacific TCD (as given by the depth of the 20°C isotherm) anomalies (bottom; negative TCD anomalies represent a shoaling of the thermocline). Annual means averaged over 5°S-5°N are shown.

Timmermann, A., S.-I. An, U. Krebs, and H. Goosse (2005), ENSO suppression due to weakening of the North Atlantic thermohaline circulation, *J. Climate*, 18, 3122–3139.

Zhang, R., and T. L. Delworth (2005), Simulated tropical response to a substantial weakening of the Atlantic thermohaline circulation. *J. Clim.*, 18(12), 1853-1860.